Coagulation of aerosol particles in turbulent flows

K. Sabelfeld* **and O. Kurbanmuradov** †

August 3, 1998

* Institute of Comp.Math. and Math. Geophysics, Russian Acad. Sciences, Lavrentieva, 6, 630090, Novosibirsk, Russia, E-mail: karl@osmf.sscc.ru and Weierstrass Institute for Applied Analysis and Stochastics, Mohrenstraße 39, D–10117 Berlin, Germany, E-mail: sabelfel@wias-berlin.de

† Scientific Technol. Center *Climate*, Turkmenian Hydrometeorology Committee, Azadi 81, 744000, Ashgabad, Turkmenistan, E-mail: seid@climat.ashgabad.su The author was supported by DFG Grant 436 TUK 17/1/98 during his visit at WIAS Institute, Berlin.

Abstract. – Coagulation of particles in turbulent flows is studied. The size distribution of particles is governed by Smoluchowski equation with random collision coefficient. The random coagulation coefficient is derived by a generalization of the approach suggested by Saffman and Turner [12]. The coagulation process is analysed in three main cases: (1) T_c, the characteristic coagulation time is much less than T_w, the characteristic Lagrangian time of the turbulent flow, (2) conversely, $T_w << T_c$, and (3), these times are of the same order: $T_w \sim T_c$. A special stochastic time is introduced which drastically simplifies the analysis of the influence of the intermittency. A detailed numerical study is given for two cases with known explicit solutions of Smoluchowski equation. The numerical analysis in the turbulent collision regime is based on the stochastic algorithm presented in the book [9] and developed in [11], [10], and [4].

1 Introduction

The coagulation processes of aerosol particles or clusters in spatially homogeneous case are governed by the Smoluchowski equation (e.g., see, [13]):

$$\frac{\partial n_l}{\partial t} = \frac{1}{2}\sum_{i+j=l} k_{ij} n_i n_j - n_l \sum_{i=1}^{\infty} k_{li} n_i \tag{1.1}$$

with the initial conditions $n_l(0) = n_l^{(0)}$, $l = 1, 2, \ldots$.

Coagulation is a process by which two particles collide and adhere, or coagulate. We use the notation: $\{l\}$-*cluster*, or l-mer, for a cluster containing l monomers (or structural units); n_i, for the number density of the $\{i\}$-*cluster*; k_{ij}, for the coagulation coefficient characterizing the collision frequencies between an $\{i\}$- and a $\{j\}$-*cluster*. We will also use the notation δ_{ij} for the Kronecker function.

Under rather general assumptions about the coagulation coefficients k_{ij} there are known existence and uniqueness results for the solution to the equation (1.1) (e.g., see [1]).

There are many different mechanisms that bring two particles to each others: Brownian diffusion, gravitational sedimentation, free molecule collisions, turbulent motion of the host gas, acoustic waves, the density, concentration and temperature gradients, particle electric charges, etc. We will deal here mainly with the case of coagulation of particles in a fully developed turbulence whose small scale statistical structure is specified by ε, the kinetic energy dissipation rate, and ν, the kinematic viscosity.

The structure of k_{ij} for different collision regimes is presented, e.g., in [13], and is well developed only in the case when there is no spatial dependence of the functions involved in the coagulation equation.

The Smoluchowski equation in the inhomogeneous case governing the coagulation of particles dispersed by a velocity field $\mathbf{v}(t, x)$ reads

$$\frac{\partial n_l(\mathbf{x}, t)}{\partial t} + \mathbf{v}(\mathbf{x}, t) \cdot \nabla n_l(\mathbf{x}, t) = \frac{1}{2}\sum_{i+j=l} k_{ij} n_i n_j - n_l \sum_{i=1}^{\infty} k_{li} n_i, \tag{1.2}$$

where $n_l(\mathbf{x}, t)$ is the concentration of clusters of size l, $l = 1, 2, \ldots$ at a point $\mathbf{x}$ at time t; $\mathbf{v}(\mathbf{x}, t)$ is the velocity of the host gas, $k_{ij} = k_{ij}(\mathbf{x}, t)$ is the coagulation coefficient. It is supposed, that the initial size tistribution is given: $n_l(\mathbf{x}, 0) = n_l^0(\mathbf{x})$.

The coagulation coefficient is determined by the flow of the host gas in the neighbourhood of the colliding particles. We assume that the flow is *incompressible* and it is *not disturbed* by the particles. Then N_{ij}, the number of collisions between the i- and j-clusters in a unit volume and unit time is defined by (e.g., see [13])

$$N_{ij}(\mathbf{x},t) = k_{ij}(\mathbf{x},t)n_i n_j = \frac{n_i n_j}{2}\int_{S_R(\mathbf{x})} |w_r(\mathbf{y})|\, dS_R(\mathbf{y}),$$

i.e.,

$$k_{ij}(\mathbf{x},t) = \frac{1}{2}\int_{S_R(\mathbf{x})} |w_r(\mathbf{y})|\, dS_R(\mathbf{y}), \tag{1.3}$$

where $R = r_i + r_j$ is the sum of the radii of colliding particles, $S_R(\mathbf{x})$ is the sphere of radius R centered at the point $\mathbf{x}$, $dS_R(\mathbf{y})$ is the surface measure at a point $\mathbf{y}$, and w_r is the radial component of the relative velocity:

$$w_r(\mathbf{y}) = \left(\mathbf{v}(\mathbf{x}+\mathbf{y},t) - \mathbf{v}(\mathbf{x},t), \frac{\mathbf{y}}{|\mathbf{y}|}\right). \tag{1.4}$$

Note that Saffman and Turner [12] described the turbulent coagulation regime in average (over the velocity fluctuations). They have defined the coagulation coefficient $\bar{k}_{ij}$ through $\langle N_{ij}\rangle$, the average of N_{ij} over the turbulent velocity fluctuations:

$$\bar{k}_{ij}(\mathbf{x},t) = \frac{1}{2}\langle\int_{S_R(\mathbf{x})} |w_r(\mathbf{y})|\, dS_R(\mathbf{y})\rangle. \tag{1.5}$$

Under the assumption that $\frac{\partial v_1}{\partial x_1}$ is normally distributed and that the velocity is isotropic in small scales, they obtained from (1.5)

$$\bar{k}_{ij}(\mathbf{x},t) \simeq 1.3(r_i + r_j)^3\sqrt{\frac{\langle\varepsilon\rangle}{\nu}}, \tag{1.6}$$

where $\langle\varepsilon\rangle$ is the average dissipation rate of the turbulent kinetic energy, and ν is the kinematic viscosity.

In our case, we deal with the random coagulation coefficient (1.3). Thus we need to evaluate the integral over the sphere. This evaluation is given in Appendix A which reads:

$$\int_{S_R(\mathbf{x})} |w_r(\mathbf{y})|\, dS_R(\mathbf{y}) = R^3\sqrt{\frac{\varepsilon}{2\nu}}\, f(\xi), \tag{1.7}$$

where f is a dimensionless universal function of a dimensionless argument ξ (see Appendix):

$$\xi = \frac{det(\hat{\tau})}{(\frac{\varepsilon}{2\nu})^{3/2}}$$

$\hat{\tau} = \|\tau_{ij}\|_{i,j=1}^3$ is the deformation tensor of the velocity $\mathbf{v}(\mathbf{x},t) = (v_1(\mathbf{x},t), v_2(\mathbf{x},t), v_3(\mathbf{x},t))$:

$$\tau_{ij} = \frac{1}{2}\left(\frac{\partial v_i}{\partial x_j} + \frac{\partial v_j}{\partial x_i}\right),$$

ε is the dissipation rate of the kinetic energy: $\varepsilon = 2\nu\sum_{ij}\tau_{ij}^2$; ν is the kinematic viscosity.

It turns out (see Appendix) that $f(\xi)$ can be approximated to within 2.3% by a constant value. Thus we have

$$k_{ij}(\mathbf{x},t) = A\sqrt{\frac{\varepsilon(\mathbf{x},t)}{\nu}}R^3, \tag{1.8}$$

where $A = 2(\pi+3)/9 \approx 1.3648$.

Remark 1.1. Note that from the expression (1.8) we find that

$$\bar{k}_{ij} = A\frac{\langle\sqrt{\varepsilon}\rangle}{\sqrt{\nu}}R^3\,. \tag{1.9}$$

Thus we see that this expression differs from (1.6). The expression (1.6) can be obtained (to within a constant factor) from (1.9) by additional assumptions on $\varepsilon(\mathbf{x},t)$, assuming for instance that ε has a lognormal distribution.

Since we study the general case of coagulation in fluctuating velocity field with k_{ij} given by (1.3), we will be able not only to find the true expectation of the solution, but also to find out when the *coagulation equation homogonization* happens. Such homogenization implies that the stochastic solution approaches the solution of the deterministic coagulation equation with $\bar{k}_{ij}$ defined in (1.9).

2 Analysis of the fluctuations in the size spectrum

Thus we deal with the Smoluchowski equation whose coagulation kernel is random:

$$\frac{\partial n_l(\mathbf{x},t)}{\partial t} + \mathbf{v}(\mathbf{x},t)\cdot\nabla n_l(\mathbf{x},t) = \frac{1}{2}\sum_{i+j=l} k_{ij}n_i n_j - n_l\sum_{i=1}^{\infty} k_{li}n_i, \tag{2.1}$$

where

$$k_{ij}(\mathbf{x},t) = A\sqrt{\frac{\varepsilon(\mathbf{x},t)}{\nu}}r_1^3(i^{1/3}+j^{1/3})^3, \tag{2.2}$$

with $A = 1.3648$; r_1 is the radius of the monomer. Here $\mathbf{v}(\mathbf{x},t)$ is a turbulent velocity field which is assumed to be incompressible, statistically homogeneous and stationary.

In Lagrangian coordinates induced by (e.g., see [6])

$$\frac{dX}{dt} = \mathbf{v}(X(t),t), \quad X(0) = \mathbf{x}_0\,, \tag{2.3}$$

the equation (2.1) reads

$$\frac{dN_l}{dt} = \frac{1}{2}\sum_{i+j=l} K_{ij}N_iN_j - N_l\sum_{i=1}^{\infty} K_{li}N_i, \quad N_l(0) = n_l^{(0)}(\mathbf{x}_0), \tag{2.4}$$

where $N_l(t) = N_l(t;\mathbf{x}_0) = n_l(X(t;\mathbf{x}_0),t)$, and

$$K_{ij}(t) = k_{ij}(X(t;\mathbf{x}_0),t) = A\sqrt{\frac{\mathcal{E}(t)}{\nu}}r_1^3(i^{1/3}+j^{1/3})^3. \tag{2.5}$$

Here $\mathcal{E}(t) = \mathcal{E}(t, \mathbf{x}_0) = \varepsilon(X(t; \mathbf{x}_0), t)$ is the Lagrangian dissipation energy rate.

To avoid unessential complications, we consider here the case when $n_l^{(0)}(\mathbf{x}) = n_l^{(0)}$ do not depend on the spatial coordinates. Then the solution is also independent of the spatial coordinates and it is governing by the homogeneous Smoluchowski equation with the coagulation coefficient (2.5).

Let us consider the following deterministic equation in dimensionless form:

$$\frac{df_l}{d\tau} = \frac{1}{2}\sum_{i+j=l}\frac{\langle K_{ij}\rangle}{\langle K_{11}\rangle} f_i f_j - f_l \sum_{i=1}^{\infty}\frac{\langle K_{li}\rangle}{\langle K_{11}\rangle} f_i, \quad f_l(0) = \frac{n_l^{(0)}}{n_0}, \tag{2.6}$$

where $n_0 = \sum_{l=1}^{\infty} l n_l^{(0)}$. It is easy to find that by introducing a new time variable τ_t defined by

$$\frac{d\tau_t}{dt} = 8An_0 r_1^3\sqrt{\frac{\mathcal{E}(t)}{\nu}} = B\sqrt{\frac{\mathcal{E}(t)}{\langle\varepsilon\rangle}}, \quad \tau(0) = 0, \tag{2.7}$$

we can express the solution to (2.4) as follows:

$$N_l(t) = n_0 f_l(\tau_t), \quad \tau_t = B\int_0^t \sqrt{\frac{\mathcal{E}(s)}{\langle\varepsilon\rangle}}\, ds. \tag{2.8}$$

Here $B = 8An_0 r_1^3\langle\sqrt{\varepsilon}\rangle/\sqrt{\nu}$.

Thus we came to a very important result: the random solution $N_l(t)$ is represented as a deterministic function of a random time τ_t. The function f_l can be obtained numerically, by the Monte Carlo [9]-[11] or a finite element method, (e.g., see [11]), hence the problem is reduced to the analysis of this random time.

In the case of incompressible homogeneous stationary velocity fields, the one-pint probability density function of the Lagrangian stochastic process $\mathcal{E}(t)$ and that of the Eulerian random field $\varepsilon(\mathbf{x}, t)$ coincide [6], therefore the function $\langle\sqrt{\mathcal{E}}\rangle$ is constant, and

$$\langle\tau_t\rangle = B\int_0^t \frac{\langle\sqrt{\mathcal{E}}\rangle}{\sqrt{\langle\varepsilon\rangle}}\, ds = B\frac{\langle\sqrt{\varepsilon}\rangle}{\sqrt{\langle\varepsilon\rangle}}t = B_1\, t, \tag{2.9}$$

where $B_1 = B\langle\sqrt{\varepsilon}\rangle/\sqrt{\langle\varepsilon\rangle}$.

Let us formulate the *coagulation equation homogenization* problem. Generally, it can be formulated as follows: when and under what conditions the fluctuation $N_l(t) - \bar{N}_l(t)$ is negligibly small where $\bar{N}_l(t)$ is the solution to the following deterministic Smoluchowski equation

$$\frac{d\bar{N}_l}{dt} = \frac{1}{2}\sum_{i+j=l}\langle K_{ij}\rangle\bar{N}_i\bar{N}_j - \bar{N}_l\sum_{i=1}^{\infty}\langle K_{li}\rangle\bar{N}_i, \quad \bar{N}_l(0) = n_l^0. \tag{2.10}$$

Let us estimate the relative fluctuation through

$$\delta_l(t) = \frac{\left\{\langle(N_l(t) - \bar{N}_l(t))^2\rangle\right\}^{1/2}}{\bar{N}_l(t)}.$$

Note that

$$\bar{N}_l(t) = n_0 f_l(\langle\tau_t\rangle) = n_0 f_l(B_1\, t). \tag{2.11}$$

The first term of the Taylor expansion gives

$$\frac{f_l(\tau+\Delta\tau)-f_l(\tau)}{f_l(\tau)}=\frac{\Delta\tau}{\lambda_l(\tau)}+\dots,$$

where

$$\lambda_l(\tau)=\frac{f_l(\tau)}{\frac{df_l(\tau)}{d\tau}}$$

is a scale characterizing the change in τ of the function $f_l(\tau)$. From this we find by (2.8),(2.11) (taking $\tau=\langle\tau_t\rangle, \Delta\tau=\tau_t'=\tau_t-\langle\tau_t\rangle$) that

$$\delta_l^2(t)=\frac{\langle(\tau_t')^2\rangle}{\lambda^2(\langle\tau_t\rangle)}+\dots. \tag{2.12}$$

Now,

$$\tau_t'=B\frac{\langle\sqrt{\varepsilon}\rangle}{\sqrt{\langle\varepsilon\rangle}}\int\limits_0^t\xi(s)\,ds=B_1\int\limits_0^t\xi(s)\,ds, \tag{2.13}$$

where

$$\xi(s)=\frac{\sqrt{\mathcal{E}(s)}-\langle\sqrt{\varepsilon}\rangle}{\langle\sqrt{\varepsilon}\rangle}. \tag{2.14}$$

By G.Taylor's formula [6] we can write

$$\langle(\tau_t')^2\rangle\simeq 2B_1^2\sigma_\xi^2T_\xi\,t,\quad \text{if}\quad t>>T_\xi,$$

where σ_ξ is the variance of ξ, and

$$T_\xi=\int_0^\infty\frac{\langle\xi(s+s')\xi(s')\rangle}{\sigma_\xi^2}ds$$

is the integral time scale of the stochastic process $\xi(s)$. Thus we obtain in (2.12)

$$\delta_l(t)\simeq\sqrt{2}\sigma_\xi\frac{\sqrt{tT_\xi}}{T_l(t)}, \tag{2.15}$$

where

$$T_l(t)=\frac{|\lambda_l(\langle\tau_t\rangle)|}{B_1}=\frac{|\bar N_l(t)|}{|\frac{d\bar N_l(t)}{dt}|}$$

is the characteristic time scale of the function $\bar N_l(t)$. From this, it is clearly seen that if $T_l(t)$ is much larger than T_ξ, the Lagrangian integral time scale of the stochastic process (2.14), then for the times $T_\xi<<t\sim T_l(t)$ the quantity δ_l behaves like $\sqrt{tT_\xi}/T_l(t)$ which implies that the fluctuations of the random functions $N_l(t)$ are small, and therefore, $\langle N_l(t)\rangle\simeq\bar N_l(t)$. Note however that $T_\xi<<t\sim T_l(t)$ is not considered as a necessary condition for ensuring that $\delta_l(t)$ is small. It was required only to derive the exact asymptotics (2.15).

It is not difficult to find that

$$\delta_l(t)\le\sqrt{2}\sigma_\xi\frac{\sqrt{tT_\xi'}}{T_l(t)}$$

provided $t << T_l^2(t)/T'_\xi$. Here

$$T'_\xi = \int_0^\infty \frac{|\langle \xi(s'+s)\xi(s')\rangle|}{\sigma_\xi^2}\, ds.$$

If $t << T_l^2(t)/T'_\xi$, then the last inequality shows that $\delta_l(t)$ is small.

Remark 2.1. Above we analysed the closeness between the expectation $\langle N_l(t)\rangle$ and the relevant deterministic function $\bar{N}_l(t)$. This closeness was controlled by the ratio $\sqrt{tT_\xi}/T_l(t)$. The same can be done for an arbitrary functional, say, $\Phi(N_l)$ (for instance, the total number of clusters, the mean cluster size, etc.). In this case the closeness between the expectation of this functional and $\Phi(\bar{N}_l)$ is controlled by $\sqrt{tT_\xi}/T_\Phi(t)$. Here

$$T_\Phi = \frac{|\bar{\Phi}(t)|}{|\frac{d\bar{\Phi}(t)}{dt}|}$$

is the characteristic time scale of the function $\bar{\Phi}(t) = \Phi(\bar{N}_l(t))$.

3 Models of the energy dissipation rate

Recall that here we deal with a spatially homogeneous, stationary and incompressible turbulent velocity field. As follows from Sect.2, the Lagrangian energy dissipation rate $\mathcal{E}(t)$ is entered the relevant Smoluchowski equation. However in the literature only the Eulerian energy dissipation rate is treated in details (e.g., see [3]). As to the Lagrangian models, to our knowledge, there are two of them: (1), The lognormal model by Pope and Chen [8], and (2), The multifractal model of Borgas and Sawford [2]. Let us describe these models.

3.1 The model by Pope and Chen $(P\&Ch)$

The model to which we will refer as $P\&Ch$ assumes that

$$\mathcal{E}(t) = \langle\varepsilon\rangle \exp(\chi(t)), \tag{3.1}$$

where $\chi(t)$ is the solution to the following stochastic differential equation [8]

$$d\chi = -\frac{1}{T_\chi}(\chi - \langle\chi\rangle) + \sigma_\chi \sqrt{\frac{2}{T_\chi}}\, dB(t), \tag{3.2}$$

where T_χ is the integral time scale of the stochastic process $\chi(t)$, while σ_χ^2 and $\langle\chi\rangle$ are its variance and mean value, respectively. Since $\chi(t)$ is a stationary Gaussian process we find from (3.1) that

$$\langle\mathcal{E}^p\rangle = \langle\varepsilon\rangle^p \exp\Big\{\frac{1}{2}p^2\sigma_\chi^2 + p\langle\chi\rangle\Big\}, \quad p > 0. \tag{3.3}$$

We used the fact that in the case considered here, the one-point statistical characteristics of the Lagrangian energy dissipation rate coincide with that of the Eulerian energy dissipation rate [6]. In particular, $\langle \mathcal{E} \rangle = \langle \varepsilon \rangle$.

Now,

$$\langle \chi \rangle = -\frac{1}{2}\sigma_\chi^2, \quad \sigma_\chi^2 = \ln\left(\frac{\langle \varepsilon^2 \rangle}{\langle \varepsilon \rangle^2}\right), \quad \langle \sqrt{\varepsilon} \rangle = \exp\left\{-\frac{\sigma_\chi^2}{8}\right\}. \tag{3.4}$$

Thus this model can be specified by the parameters: $\langle \varepsilon \rangle, \langle \varepsilon^2 \rangle$, and T_χ, or alternatively, by $\langle \varepsilon \rangle, \langle \sigma_\chi^2 \rangle$, and T_χ. Note that in [8], the last variant was used, with $\sigma_\chi = 1$, and $T_\chi = 0.9T_w$, where T_w is the Lagrangian time scale of the vertical velocity fluctuations.

We will use both these variants. In the first variant, we will use the following relation (e.g., see [3] and [2]):

$$\frac{\langle \varepsilon^2 \rangle}{\langle \varepsilon \rangle^2} = \left(\frac{T_w}{\tau_\eta}\right)^\mu, \tag{3.5}$$

where $\tau_\eta = \sqrt{\nu/\langle \varepsilon \rangle}$ is the Kolmogorov internal time scale, and μ is the intermittency parameter ($\mu = 0.2 \div 0.3$).

Remark 3.1.

By the definition of ξ (see (2.14)) we can find, using (3.3) that

$$\sigma_\xi^2 = \frac{\langle \varepsilon \rangle}{\langle \sqrt{\varepsilon} \rangle^2}\left(1 - \exp\{-\frac{\sigma_\chi^2}{4}\}\right).$$

The integral time scale T_ξ can be estimated from the following arguments.

Let $\zeta(t) = \exp\{\chi(t)\}$, where $\chi(t)$ is the Ornstein-Uhlenbeck process defined by (3.2). Then the following approximate relation holds [8]:

$$T_\zeta = T_\chi\Big(1 - \frac{2}{9}\sigma_\chi^2\Big),$$

where T_ζ is the integral time scale of the process $\zeta(t)$. This approximation is applicable if $\sigma_\chi^2 \le 2$. From this we find that

$$T_\xi = T_\chi\Big(1 - \frac{1}{18}\sigma_\chi^2\Big).$$

3.2 The model by Borgas and Sawford ($B\&S$)

In this model, there are three input parameters: $\langle \varepsilon \rangle, T_w$ and N_ε, a positive integer. The model can be described as follows. Let η, ρ, δ be independent random numbers constructed as

$$\eta = \begin{cases} a & \text{with probability} \quad \lambda \\ b & \text{with probability} \quad 1-\lambda, \end{cases}$$

$$\rho = \begin{cases} a' & \text{with probability} \quad \lambda' \\ b' & \text{with probability} \quad 1-\lambda', \end{cases}$$

$$\delta = \begin{cases} 0 & \text{with probability} \quad 0.5 \\ 1 & \text{with probability} \quad 0.5, \end{cases}$$

where $a = 0.7528$, $b = 0.3536$, $a' = 0.3951$, $b' = 0.1474$, $\lambda = \sqrt{a}$, $\lambda' = 1 - \sqrt{b}$.

Let us define a subdivision of the interval $\Delta = [0, T_w)$. First, let $\Delta_1^{(0)} = \Delta$. Then, for a positive integer i we construct a uniform subdivision of Δ into 2^i subintervals: $\Delta_1^{(i)}, \Delta_2^{(i)}, \ldots, \Delta_{2^i}^{(i)}$. The interval $\Delta_j^{(i)}$ is divided in two equal subintervals: the left, $\Delta_j^{(i)'}$, and the right subinterval $\Delta_j^{(i)''}$.

The stochastic process $\mathcal{E}(t)$ on the interval $\Delta = [0, T_w)$ will be constructed recursively in $N_\varepsilon + 1$ steps.

Step (0): Put $\mathcal{E}_0(t) \equiv \langle \varepsilon \rangle$, $t \in \Delta_1^{(0)}$.
Step (1): Simulate a triple $(\eta_1^{(0)}, \rho_1^{(0)}, \delta_1^{(0)})$ of independent random numbers as described above. Then define

$$\mathcal{E}_1(t) = \begin{cases} 2\mathcal{E}_0(t)[\delta_1^{(0)}\eta_1^{(0)} + (1 - \delta_1^{(0)})\rho_1^{(0)}], & \text{if } t \in \Delta_1^{(0)'} \\ 2\mathcal{E}_0(t)[(1 - \delta_1^{(0)})\eta_1^{(0)} + \delta_1^{(0)}\rho_1^{(0)}], & \text{if } t \in \Delta_1^{(0)''}. \end{cases}$$

Step (i): Let $(\eta_j^{(i-1)}, \rho_j^{(i-1)}, \delta_j^{(i-1)})$, $j = 1, \ldots, 2^{i-1}$ be independent samples. In the interval $\Delta_j^{(i-1)}$ $(j = 1, \ldots, 2^{i-1})$ we define

$$\mathcal{E}_i(t) = \begin{cases} 2\mathcal{E}_{i-1}(t)[\delta_j^{(i-1)}\eta_j^{(i-1)} + (1 - \delta_j^{(i-1)})\rho_j^{(i-1)}], & \text{if } t \in \Delta_j^{(i-1)'} \\ 2\mathcal{E}_{i-1}(t)[(1 - \delta_j^{(i-1)})\eta_j^{(i-1)} + \delta_j^{(i-1)}\rho_j^{(i-1)}], & \text{if } t \in \Delta_j^{(i-1)''}. \end{cases}$$

etc., till $i = N_\varepsilon$. Finally, set $\mathcal{E}(t) = \mathcal{E}_{N_\varepsilon}(t)$.

The following relations are known for this model [2]:

$$\langle \mathcal{E}^2(t) \rangle = \langle \varepsilon \rangle^2 \left(\frac{T_w}{\tau_\eta} \right)^\mu,$$

where $\mu = 0.294$, and $\tau_\eta = 2^{-N_\varepsilon} T_w$ is the inner time scale of the model. In addition, the integral time scale of $\mathcal{E}(t)$ satisfies

$$T_\mathcal{E} \approx C_\varepsilon T_w \left(\frac{T_w}{\tau_\eta} \right)^{-\mu},$$

where C_ε is a constant which does not depend on the subdivision.

In conclusion let us make some remarks concerning the two described models.
1. The probability density function (pdf) of the model $P\&Ch$ is lognormal with a heavy tail, while for the pdf of the model $B\&S$ this is not the case.
2. The correlation function of the model $P\&Ch$ is approximately exponentially decaying [8]. The correlation function of the $P\&Ch$ model it is a power function.
3. The model $P\&Ch$ is much more convenient in numerical simulations. However it does not involve the dependence on the Reynolds number in contrast to the model $B\&S$.

4 Monte Carlo simulation for Smoluchowski equation in a stochastic coagulation regime.

In Section 2 we have suggested theoretical analysis which provides qualitatively estimations (see (2.15)) of the difference between the true expectations of the solutions to stochastic Smoluchowski equation and the solutions of the relevant deterministic equations. These estimations show that two main cases may occur: (1) this difference is small which happens when $\sqrt{tT_\xi} << T_l(t)$, and (2), this difference is not small if $\sqrt{tT_\xi} \simeq T_l(t)$. However, since the function $T_l(t)$ is generally very complicated, this criterion is not easy applied in practice. Therefore, we first investigate the case of a model Smoluchowski equation which has an explicit solution. In this case the criterion is also explicitly verified.

Let us consider the following Smoluchowski equation of the type (2.4) with the coagulation coefficient

$$K_{ij} = \frac{\beta}{n_0}\sqrt{\frac{\mathcal{E}(t)}{\nu}}\,(i+j), \tag{4.1}$$

with the initial condition $N_l(0) = n_0\delta_{l1}$. Here $\beta = \frac{4}{3}\pi r_1^3 n_0$ is a dimensionless parameter, r_1 is the radius of the monomer, n_0 is the initial number of monomers. Note that β has a clear physical meaning: it is the total volume occupied by monomers in a unit volume.

As described in Sect.1, our solution can be represented as

$$N_l(t) = n_0 f_l(\tau_t), \quad \tau_t = \frac{\beta}{\tau_\eta}\int\limits_0^t \sqrt{\frac{\mathcal{E}(s)}{\langle\varepsilon\rangle}}\,ds, \tag{4.2}$$

where τ_t is the internal Kolmogorov time scale, and $f_l(\tau)$ is a dimensionless function of the dimensionless time τ satisfying the equation

$$\frac{df_l}{d\tau} = \frac{1}{2}\sum_{i+j=l}(i+j)f_i f_j - f_l\sum_{i=1}^{\infty}(l+i)f_i, \quad f_l(0) = \delta_{l1}. \tag{4.3}$$

Let us also consider the deterministic function $\bar{N}_l(t)$ which is the solution to (2.10) with the coagulation coefficients $\langle K_{ij}\rangle$ where K_{ij} is given by (4.1) and with the initial distribution $\bar{N}_l(0) = n_0\delta_{l1}$. Here we have also

$$\bar{N}_l(t) = n_0 f_l(\langle\tau_t\rangle), \quad \langle\tau_t\rangle = \frac{\beta}{\tau_\eta}\frac{\langle\sqrt{\varepsilon}\rangle}{\sqrt{\langle\varepsilon\rangle}}t\,. \tag{4.4}$$

In this case, the exact solution to (4.3) is known [13]:

$$f_l(\tau) = n_0\frac{l^{l-1}}{l!}[b(\tau)]^{l-1}\exp\{-\tau - lb(\tau)\}, \quad b(\tau) = 1-\exp(-\tau). \tag{4.5}$$

Along the solution itself, we will be interested in the following functionals:
(1) Total number of clusters:

$$\Sigma(t) = \sum_{l=1}^{\infty} N_l(t), \tag{4.6}$$

(2) Mean cluster size:

$$\Lambda(t) = \frac{1}{\Sigma(t)} \sum_{l=1}^{\infty} l N_l(t). \tag{4.7}$$

In the case considered here these functions are explicitly known:

$$\Sigma(t) = n_0 \exp(-\tau_t), \quad \Lambda(t) = \exp(\tau_t). \tag{4.8}$$

In the deterministic case, these functionals of the solutions to the deterministic Smoluchowski equation are

$$\begin{aligned} \bar{\Sigma}(t) &= \sum_{l=1}^{\infty} \bar{N}_l(t) = n_0 \exp(-\langle\tau_t\rangle) = n_0 \exp(-\frac{t}{T_c}), \\ \bar{\Lambda}(t) &= \frac{1}{\bar{\Sigma}(t)} \sum_{l=1}^{\infty} l \bar{N}_l(t) = \exp(\langle\tau_t\rangle) = \exp(t/T_c), \end{aligned} \tag{4.9}$$

where

$$T_c = \frac{\tau_\eta}{\beta} \frac{\sqrt{\langle\varepsilon\rangle}}{\langle\sqrt{\varepsilon}\rangle} \tag{4.10}$$

is an integral time scale of the coagulation process. Here $\tau_\eta = \sqrt{\frac{\nu}{\langle\varepsilon\rangle}}$ is the internal Kolmogorov time scale. In the calculations we take $\langle\varepsilon\rangle = 100$, $T_w = 10$, $\nu = 0.17$. *We use everywhere the* **CGS** *units.*

We will use the relation:

$$\langle\varepsilon^2\rangle = \langle\varepsilon\rangle^2 \left(\frac{T_w}{\tau_\eta}\right)^{\mu}, \tag{4.11}$$

where the intermittency parameter is chosen as $\mu = 0.25$.

Throughout this section (except for Sect.4.4), the stochastic process $\mathcal{E}(t)$ will be simulated according to the model $P\&Ch$. The parameters were chosen as follows: $\langle\varepsilon\rangle = 100$, with the relevant value of $\langle\varepsilon^2\rangle$ given by (4.11), and $T_\chi = 0.9 T_w$.

In the process of coagulation governed by the random Smoluchowski equation (2.4) with the coagulation coefficient (4.1) two main time scales are involved: T_w, the Lagrangian time scale of the velocity fluctuations, and T_c, the integral time scale of the coagulation process. It is therefore very convenient to introduce a number γ characterising the rate of the coagulation: $\gamma = T_w/T_c$. We will consider four cases:

High rate of coagulation, if $\gamma \sim 10$,
Moderate high rate, if $\gamma \sim 1$,
Moderate low rate, if $\gamma \sim 0.1$,
Low rate, if $\gamma \sim 0.01$.

Here and in what follows, we use the notation $a \sim b$ to indicate that $a = C\,b$ where C is a constant of order 1. The radius of the monomer is taken as $r_1 = 10^{-4}$.

We have chosen the values $n_0 = 10^{10}$, $n_0 = 10^9$, $n_0 = 10^8$, and $n_0 = 10^7$ which correspond to the four coagulation rates mentioned above.

4.1 The total number of clusters and the mean cluster size

In this section we present the numerical analysis for $\Sigma(t)$ and $\Lambda(t)$.

Let us denote by $\delta_\Sigma(t)$ the relative difference between the average of the stochastic function $\Sigma(t)$ and the deterministic function $\bar{\Sigma}(t)$:

$$\delta_\Sigma(t) = \frac{\langle \Sigma(t) \rangle - \bar{\Sigma}(t)}{\bar{\Sigma}(t)}.$$

In Fig.1, this quantity (lower curve) is shown for the case of moderate high rate of coagulation ($\gamma = 0.86$) as a function of the dimensionless time $\tau = t/T_c$. For convenience, we plot also the ratio $\sqrt{T_w t}/T_c = \sqrt{\gamma\tau}$ (upper curve).

It is seen from this curves, that the deterministic and stochastic cases do not much differ if $\tau \leq 1$ (to within 10%). After a certain time instant τ_0 the function $\sqrt{\gamma\tau}$ is close to 1 which indicates that after this time the difference becomes large.

In Fig.2 the same curves are plotted in the case of moderate low rate of coagulation ($\gamma = 0.086$). It is seen that the time instant $\tau_0 \sim 1/\gamma$ happens later, between 6 and 8.

Thus even in the case of moderate low rate of coagulation the difference becomes large after the dimensional time $t_0 \sim \tau_0 T_c = T_c^2/T_w$.

The expectation of the mean cluster size $\langle \Lambda \rangle$ is shown in Fig.3 in the case of moderate high rate of coagulation ($\gamma = 0.86$). Two upper curves were obtained by Monte Carlo averaging over 10^4 and 10^5 samples which shows that the statistical error is small enough. The lower curve is the deterministic function $\bar{\Lambda}(\tau)$. It is seen that after the time instant $\tau_0 \sim 1$ the difference starts to increase rapidly, and around $\tau = 8$ it reaches two orders of magnitude. Qualitatively the same picture was obtained for $\gamma = 0.085$.

For the low rate of coagulation ($\gamma = 0.0085$) the difference between the stochastic and deterministic functions is practically eliminated, see Figs.4 and 5.

Thus in the case of these two functions the stochastic description can be well approximated by deterministic equation for low rate of coagulation at times up to several number of characteristic coagulation times T_c. The lower the coagulation rate, the wider is the interval where the coagulation equation homogenization takes place.

It should be noted that this conclusion is made for these two specific functions, the total number of clusters and the mean cluster size. The situation can be drastically changed if the solution itself is considered. Let us consider some examples.

4.2 The functions $N_3(t)$ and $N_{10}(t)$

In Fig.6. we present $\langle N_3(t) \rangle / n_0$, the normalized concentration of 3-mers as a function of dimensional time for the moderate high rate of coagulation ($\gamma = 0.86$). The upper curve is obtained by the Monte Carlo averaging over $N = 10^4$ samples, the lower curve is the function $\bar{N}_3(t)/n_0$. Note that the difference is seen for all times though it is much larger for times $t \sim 5T_c$, $T_c = 11.68$ sec. The difference is even more pronounced for the 10-mers.

The picture is different in the case of low rate of coagulation ($\gamma = 0.0086$). As shown in Fig.7, the difference is seen only for times up to $\sim T_c = 1168$ sec. After this time instant the curves are very close. To explain such behaviour we plot here in the upper

picture also T_{10}, the characteristic time scale of coagulation for 10-mers defined in Sect.4. From (2.15) it follows that the smaller $T_{10}(t)$, the larger the relative difference between the stochastic and deterministic cases.

To see a more detailed picture for clusters of different sizes, we turn to the size spectrum, i.e., the size distribution density $N_l(t)$.

4.3 The size spectrum N_l for different time instances

First we consider the case of low coagulation rate ($\gamma = 0.0086$), $T_c = 1168$.

In Figs.8-10 we plot the size spectrum at the time $t = T_w = 10$ sec, $t = 10T_w = 100$ sec, and $t = 100T_w = 1000$ sec, respectively. The upper curve is obtained by Monte Carlo calculations, the lower curve is the deterministic function $\bar{N}_l/n_0$. The difference becomes rapidly larger with the growth of the cluster size. Note that the larger the time instances the wider is the size interval where the difference between the stochastic and deterministic cases is small (e.g., compare Fig.8 and Fig.10). In calculations (which we do not show here) made for $t = 500T_w$ the curves are close up to the 500-mers.

Let us consider the case of moderate low coagulation rate ($\gamma = 0.086$, $T_c = 116.8$). The pictures 11-13 present the same curves for $t = T_w, 10T_w$ and $100T_w$, respectively. Here we see qualitatively the same picture with one difference that in the case $t = 100T_w$ the difference between the curves holds for all the sizes.

It is interesting to note that for $t = 500T_w$ this difference is increased about three times for all the sizes up to $l = 500$ (these results are not shown here).

The case of the moderate high coagulation rate ($\gamma = 0.86$, $T_c = 11.68$): Figs.14 and 15 correspond to the cases $t = T_w$ and $t = 10T_w$, respectively. In this case the curves are different for all the considered sizes (except for small sizes in Fig.14). The difference becomes even more pronounced in the case of high coagulation rate ($\gamma = 8.6$, $T_c = 1.17$) (see Figs.16 and 17).

4.4 Comparative analysis for two different models of the energy dissipation rate

As mentioned in Sect.3, the models $B\&S$ and $P\&Ch$ differ in certain aspects, in particular, the tails of the distributions are quite different. Therefore, one may expect that this will lead to a change of the numerical results of the previous section. We compare in this section the results for both models with common mean value. In the model $B\&S$ we take $T_w = 30$, $N_\varepsilon = 8$, and the mean dissipation rate $\langle\varepsilon\rangle$ is determined from the relation $\tau_\eta = 2^{-N_\varepsilon} T_w = (\nu/\langle\varepsilon\rangle)^{1/2}$. For $\nu = 0.17$ we have $\langle\varepsilon\rangle = 12.38$.

In the model $P\&Ch$ we choose the parameters from the following arguments. The mean is taken the same, $\langle\varepsilon\rangle = 12.38$; $T_\chi = 0.9T_w$, and the variance σ_χ^2 was taken equal to the variance of the random variable $\chi = \ln(\mathcal{E}/\langle\varepsilon\rangle)$ where $\mathcal{E}$ is taken from the model $B\&S$. This results in $\sigma_\chi = 1.7$.

First we show the results for the mean cluster size $\Lambda(t)$. The two models give similar results for low coagulation rates ($\gamma \sim 1$), see the relevant results in the previous section.

For high coagulation rates the models give essentially different results. In Fig.18 the expectation of the mean cluster size was obtained for the model $P\&Ch$ with $N = 4000$ and $N = 40000$ samples. The lower curve is the deterministic function $\bar{\Lambda}(t)$.

The difference between the two upper curves should be additionally explained. Simple analysis of the explicit expression of the expectation $\langle\Lambda(\tau_t)\rangle$ shows that it behaves essentially different at small and large times. For large (compared with T_χ) times the distribution of τ_t is approximately Gaussian, and the expectation $\langle\Lambda(\tau_t)\rangle = \langle\exp\{\tau_t\}\rangle$ is well defined. However for small times, the pdf of τ_t has a heavy tale, since τ_t is proportional to $\sqrt{\mathcal{E}(0)}$, $\mathcal{E}(0)$ being lognormal distributed. Therefore, the expectation $\langle\Lambda(\tau_t)\rangle$ tends to infinity. This explains why the Monte Carlo calculations with $N = 40000$ and 4000 samples are so different, thus not providing stable results.

The model $B\&S$ gives essentially different results, see Fig.19. Here we have very stable Monte Carlo results of $\langle\Lambda(\tau_t)\rangle$, and the deviation from the deterministic case is clearly seen though not so large.

As we will see, this is a general situation: the lognormal model $P\&Ch$ leads to a larger difference between the stochatic and deterministics cases.

Let us turn to more fine functions, namely we present the results for monomers, 10-mers and 50-mers.

In Fig.20 (high coagulation rate, $\gamma \sim 8$) the difference between the deterministic and stochastic cases (for monomers) becomes large for the model $P\&Ch$ after a couple of seconds, while for the $B\&S$ model the difference is small for the times up to 30 sec. It becomes even smaller in the case of lower ($\gamma \sim 2.5$) coagulation rate (see Fig.21).

For 10- and 50-mers the general picture is the same: the lognormal model $P\&Ch$ leads to a larger difference between the stochatic and deterministics cases (see Figs.22-23). Note that the difference between the deterministic and stochastic cases behaves here not monotonic: for small times the deterministic solution is larger, then at a small time interval it is smaller, and then it is again larger.

Let us consider the whole size spectrum. From Fig.24 (high coagulation rate, $\gamma \sim 8$) and Fig.25 (moderate high coagulation rate, $\gamma \sim 2.5$) we can see that here both models lead to a difference between the deterministic and stochastic cases, but again, this difference is much larger for the model $P\&Ch$.

5 The case of coagulation coefficient with no dependence on the cluster size

The case of a coagulation coefficient with no dependence of the cluster size may be usefull in the study of the case of turbulent coagulation coefficient generalized by [7]. Therefore, it is interesting to study this case in more details, since it provides explicit expression of the solution.

Thus we assume that all the parameters remain the same as in the previous section, with the only one difference, namely, the term $i + j$ is replaced with 1:

$$K_{ij} = \frac{\beta}{n_0}\sqrt{\frac{\mathcal{E}(t)}{\nu}}. \tag{5.1}$$

The exact solution to the Smoluchowski equation (2.6) in this case has the form:

$$f_l(\tau) = \frac{b^{l-1}}{(1+b)^{l+1}}, \quad b = b(\tau) = \frac{\tau}{2}. \tag{5.2}$$

In calculations, we consider three cases of coagulation rate: $\gamma \sim 10$, 1 and 0.1 which correspond to the initial number density $n_0 = 5.10^9$, 5.10^8, and 5.10^7, respectively.

The results show that for high and moderate high coagulation rates (see Fig.26, and Figs.29-32) at the times $t \sim T_c$ the difference between the stochastic and deterministic cases is large. In contrast to the case when $K_{ij} \sim (i+j)$, here even for the high coagulation rate at the times $t >> T_c$ the difference between the stochastic and deterministic cases is very small (see Figs. 27-28). This can be explained by comparing the scales $T_l(t)$ of these two cases. From the exact solutions (4.5) and (5.2) we find that for large times, $f_l(\tau) \sim \exp(-\tau)$ and $f_l(\tau) \sim 1/\tau^2$, respectively. Hence, if $t >> T_c$, then $T_l(t) \simeq T_c$ and $T_l(t) \simeq t$, respectively. Therefore, from the relation (2.15) we conclude that in the case when the coagulation coefficient does not depend on i and j, the difference between the stochastic and deterministic cases is small for all cases of γ if the time is much larger than both the characteristic time scales T_w and T_c.

6 Monte Carlo simulation of coagulation processes in turbulent coagulation regime

Let us study the difference between the deterministic and stochastic cases in the case of turbulent coagulation regimes.

We will use the coefficient derived in Appendix (see formula (2.5)):

$$K_{ij}(t) = A\sqrt{\frac{\mathcal{E}(t)}{\nu}} r_1^3 (i^{1/3} + j^{1/3})^3. \tag{6.1}$$

It should be noted that both in our and Turner and Saffman's considerations it was assumed that the statistical structure of the flow is considered undesturbed by the particles. This implies that the radii of the particles can not much differ, say the radii ratio is not larger than 3. In [7] a generalization is presented which is free of this restriction. The authors [7] derived a correction factor E to the coagulation coefficient of Turner and Saffman, namely $E = 7.5(\rho_2/\rho_1)^2$ where ρ_1 and ρ_2 are the larger and smaller radius of the colliding particles. Thus if $i/3 > j$, then we put

$$K_{ij}(t) = E_{ij}\, A\sqrt{\frac{\mathcal{E}(t)}{\nu}} r_1^3 (i^{1/3} + j^{1/3})^3, \tag{6.2}$$

where

$$E_{ij} = 7.5 \left(\frac{j}{i}\right)^2, \quad j = \min\{i,j\},\ i = \max\{i,j\}. \tag{6.3}$$

Otherwise, $E_{ij} = 1$.

Since the exact solutions to Smoluchowski equation with the kernels (6.1) and (6.2) are not known, we used the Monte Carlo stochastic particle method developed in [9]-[11] and recently extended to the inhomogeneous case [5].

It is interesting to note that the behaviour of the turbulent coagulation coefficient (6.1) considered as a function of i and j is close to the case $K_{ij} \sim i + j$ treated in details in Sect.4. while the corrected turbulent coagulation coefficient (6.2) is close to the case $K_{ij} \sim const$ treated in Sect.5 in the sense that the relevant solutions behave qualitatively similar, as we will see later.

We present calculations both for the coefficient (6.1) and (6.2). We used here the model $P\&Ch$ with the parameters chosen as in Sect.4.

The calculations were carried out for three coagulation rates: (1) high coagulation rate, $\gamma = 11.15$, $(n_0 = 5.\,10^9, T_c = 0.89)$, (2) moderate high coagulation rate, $\gamma = 1.11$, $(n_0 = 5.\,10^8, T_c = 8.9)$, (3) moderate low coagulation rate, $\gamma = 0.11$, $(n_0 = 5.\,10^7, T_c = 89)$, where

$$T_c = \frac{1}{B_1} = \frac{\tau_\eta}{8An_0r_1^3}\frac{\sqrt{\langle\varepsilon\rangle}}{\langle\sqrt{\varepsilon}\rangle}.$$

The radius of the monomer was taken the same as in previous calculations: $r_1 = 10^{-4}$ cm.

Let us study the difference between the deterministic and stochastic cases for the coagulation coefficient (6.1). In Fig.35 the normalized concentration of 10-mers is shown as a function of time, for high coagulation rate. As in the case $K_{ij} \sim (i + j)$, (see Fig.22), the expectation differs from the deterministic solution both for small and large time instances. This picture remains true in the case of moderate high coagulation rate, but the difference becomes smaller for large times. Again, this situation is similar to that observed in the case of $K_{ij} \sim (i + j)$ (see Fig.7).

A qualitatively analogy remains true also for other functions like the expectation of the mean cluster size and the total number of clusters.

We turn to the case of the corrected coagulation coefficient (6.2).

In this case we plot in Figs.37-39 the normalized concentration of 10-mers as a function of time for the moderate low, moderate high, and high coagulation rates, respectively. At small times ($t \leq T_c$) the curves behave similar to the case with the coagulation coefficient (6.1), see Figs.35-36. However for the times $t \geq T_c$, this is not the case, and the curves in Figs.37-39 look rather similar to the relevant curves for the case when the coagulation coefficient does not depend on i and j (see Figs.32-33).

Thus we conclude that the case of turbulent coagulation coefficient (6.1) (without correction E_{ij}), is qualitatively described by the case $K_{ij} \sim (i + j)$. Therefore, the detailed analysis given in Sect.4 may be usefull in this case. The case of corrected coagulation coefficient (6.2) can be qualitatively analysed on the basis of the calculation results presented in Sect.5.

7 Conclusion

The coagulation processes in a turbulent regime are studied. The main purpose of the paper is to distinguish between an averaged description and discription in a fluctuating dissipation rate of the kinetic turbulent energy $\mathcal{E}(t)$. The averaged description was proposed by Saffman and Turner [12], and the coagulation coefficient in a fluctuating $\mathcal{E}(t)$ is given in the present paper by formula (2.2). It turns out that in many cases these two descriptions lead to essentially different average solutions. However it is also often the case when both description give close results. This last case called here *coagulation equation homogenization* is studied in details, and conditions under which the homogenization takes place are derived.

We have analysed two cases of turbulent coagulation coefficient: (1), the coefficient (6.1) which is derived under assumption that the particles do not disturb the flow; (2), the coefficient (6.2) which involves a correction coefficient (given in [7]; the correction accounts for the structure of flow around the bigger particle).

In the case (1), for the high and moderate high coagulation rates when $\gamma = T_w/T_c \sim 1$ (T_w is the characteristic Lagrangian time scale of the velocity fluctuations, and T_c is the characteristic time scale of the coagulation process) then the stochastic and deterministic descriptions lead to different behaviour of the size spectrum. In the moderate low and low coagulation rates both descriptions lead to close results only for times well within the interval $(T_c, T_c/\gamma)$.

In the case (2), the difference is pronounced tipically only in the initial time interval $(0, g\,T_c))$, where the dimensionless constant $g \sim 1$.

Two different models of the fluctuated dissipation rate of turbulent energy, the lognormal model $P\&Ch$ and the multifractal model $B\&S$ are used in our calculations. These models give qualitatively close results, however the lognormal model leads as a rule to larger difference between the stochastic and deterministic descriptions.

It should be noted that the turbulence was assumed to be spatially homogeneous and stationary in time. Besides, we studied only the coagulation mechanism due to relative motion of colliding particles in a turbulent velocity field. Thus we have not included the inertion of partices, the Brownian diffusion, gravitational sedimentation, etc. It is believed that the approach presented in this paper can be extended to more general sitations cited above.

8 Appendix. Derivation of the coagulation coefficient

Let us evaluate the coagulation coefficient

$$k_{ij}(\mathbf{x},t) = \frac{1}{2}\int_{S_R(\mathbf{x})} |w_r(\mathbf{y})|\, dS_R(\mathbf{y}) \tag{8.1}$$

under the assumptions: the velocity $\mathbf{v}(\mathbf{x},t)$ is incompressible, and the characteristic spatial scale of the velocity field is much larger than the size of the coagulating particles. First, expand the relative velocity:

$$\begin{aligned} v_i(\mathbf{x}+\mathbf{y},t) - v_i(\mathbf{x},t) &= \sum_{j=1}^{3} \frac{\partial v_i(\mathbf{x},t)}{\partial x_j}\, y_j + \dots \\ &= \frac{1}{2}\sum_{j=1}^{3}\Big\{\frac{\partial v_i(\mathbf{x},t)}{\partial x_j} + \frac{\partial v_j(\mathbf{x},t)}{\partial x_i}\Big\}\, y_j + \frac{1}{2}\sum_{j=1}^{3}\Big\{\frac{\partial v_i(\mathbf{x},t)}{\partial x_j} - \frac{\partial v_j(\mathbf{x},t)}{\partial x_i}\Big\}\, y_j + \dots \end{aligned} \tag{8.2}$$

where we omit the terms higher than the linear ones. Now, the radial component is expressed through the scalar product:

$$\begin{aligned} w_r(\mathbf{y}) \;&=\; (\mathbf{v}(\mathbf{x}+\mathbf{y},t) - \mathbf{v}(\mathbf{x},t), \frac{\mathbf{y}}{|\mathbf{y}|}) = \sum_j \sum_i \frac{\partial v_i(\mathbf{x},t)}{\partial x_j}\,\frac{y_j y_i}{|\mathbf{y}|} + \dots \\ &= \sum_i \sum_j \tau_{ij} \frac{y_i y_j}{|y|} + \dots . \end{aligned} \tag{8.3}$$

Then we calculate the integral using the relevant coordinate system (by a rotation to the principal axes of $\hat{\tau}$)

$$\frac{1}{2}\int\limits_{S_R(\mathbf{x})} |\sum_{ij}\tau_{ij}\frac{y_i y_j}{|y|}|\, dS_R(\mathbf{y}) = \frac{1}{2R}\int_{S_R(\mathbf{x})} |\lambda_1 y_1^2 + \lambda_2 y_2^2 + \lambda_3 y_3^2|\, dS_R(\mathbf{y})$$
$$= \frac{R^3}{2}\sqrt{\lambda_1^2+\lambda_1^2+\lambda_1^2}\int\limits_{S_1(\mathbf{x})} |\mu_1 y_1^2 + \mu_2 y_2^2 + \mu_3 y_3^2|\, dS_1(y),$$

where $\lambda_1, \lambda_2, \lambda_3$ are the eigen-values of the strain tensor $\hat{\tau}$, and $\mu_i = \lambda_i/\sqrt{\lambda_1^2+\lambda_1^2+\lambda_1^2}$, $i = 1, 2, 3$. Thus,

$$k_{ij} = \frac{R^3\sqrt{\lambda_1^2+\lambda_1^2+\lambda_1^2}}{2}\int\limits_{S_1} |\mu_1 y_1^2 + \mu_2 y_2^2 + \mu_3 y_3^2|\, dS_1(y).$$

The last integral depends on one parameter since $\mu_1^2+\mu_2^2+\mu_3^2 = 1$, and, by incopressibility, $\mu_1 + \mu_2 + \mu_3 = 0$.

Thus we have to evaluate the integral over the sphere $S_1(\mathbf{x})$ for the whole region of this parameter. Let us treat this problem as follows.

The intersection of $\mu_1^2 + \mu_2^2 + \mu_3^2 = 1$ and $\mu_1 + \mu_2 + \mu_3 = 0$ is a circle which can be parametrized through

$$\mu_1 = \frac{1}{\sqrt{2}}\cos\theta + \frac{1}{\sqrt{6}}\sin\theta,\ \mu_2 = -\frac{1}{\sqrt{2}}\cos\theta + \frac{1}{\sqrt{6}}\sin\theta,\ \mu_3 = -\frac{2}{\sqrt{6}}\sin\theta,$$

where $\theta \in [0, 2\pi)$. Consequently,

$$\frac{1}{2}\int\limits_{S_1} |\mu_1 y_1^2 + \mu_2 y_2^2 + \mu_3 y_3^2| dS_1 = 2\pi E_\omega |\mu_1(\theta)\omega_1^2 + \mu_2(\theta)\omega_2^2 + \mu_3(\theta)\omega_3^2| \equiv F(\theta),$$

where $\omega = (\omega_1, \omega_2, \omega_3)$ is a random unit isotropic vector, E_ω means the expectation taken over the vector ω.

Monte Carlo calculations of the expectation shows that the function $F(\theta)$ has its maximum at $\theta = 0$ and the minimum at $\theta = \pi/2$. Explicit expression of the integral at these points gives $F(0) = 8/3\sqrt{2}$, $F(\pi/2) = 8\pi/9\sqrt{2}$. Thus

$$\frac{8}{3\sqrt{2}} \le \frac{1}{2}\int\limits_{S_1} |\mu_1 y_1^2 + \mu_2 y_2^2 + \mu_3 y_3^2|\, dS_1(y) \le \frac{8}{3\sqrt{2}}\frac{\pi}{3}.$$

Therefore we can approximate the integral by a constant which is the mean of $F(0)$ and $F(\pi/2)$ (to within 2.3%). This yields

$$K_{ij} = \frac{1}{2}\int_{S_R(\mathbf{x})} |w_r(\mathbf{y})|\, dS_R(\mathbf{y}) \simeq A\sqrt{\frac{\varepsilon}{\nu}}(r_i + r_j)^3 \tag{8.4}$$

with $A = 2(\pi+3)/9 \approx 1.3648$.

Acknowledgement. The authors thank A.A. Kolodko for her interest and collaboration while discussing this work. She kindly made the Monte Carlo calculations in the case of Smoluchowski equation with the kernels (6.1) and (6.2).

This work is partially supported by Grants INTAS-RFBR N 95-IN-RU-726 and the Nato Linkage Grant N 971664.

References

[1] J.M. Ball, J. Carr. The discrete coagulation-fragmentation equations: existence, uniqueness and density concentration. *J. Stat. Phys.* (1990), **61**, 203–234.

[2] Borgas M.S. and Sawford B.L. Stochastic equations with miltifractal random increments for modeling turbulent dispersion. *Phys. Fluids* (1994), **6**, N2, 618–633.

[3] Frisch U. *Turbulence.* Cambridge University Press, 1996.

[4] Kolodko A.A. and Wagner W. Convergence of a Nanbu type method for Smoluchowski equation. *Monte Carlo Methods and Applications* (1997), **3**, 4, 255–273.

[5] Kolodko A.A., Sabelfeld K.K. and Wagner W. A stochastic method for solving Smoluchowski coagulation equation. In press.

[6] Monin A.S. and Yaglom A.M. *Statistical Fluid Mechanics.* Vol. **2** M.I.T. Press, Cambridge, Massachusets, 1975.

[7] Pnueli, C. Gutfinger, and M. Fichman. A Turbulent-Brownian model for aerosol coagulation. *Aerosol Science and Technology.* (1991), **14**, 201-209.

[8] Pope S.B. and Chen Y.L. The velocity-dispersion probability density function model for turbulent flows. *Phys. Fluids A* (1990), **2**, N.8, 1437–1449.

[9] Sabelfeld K.K. *Monte Carlo Methods in Boundary Value Problems.* Springer–Verlag. Heidelberg–New York–Berlin, 1991.

[10] Sabelfeld K. K. and Kolodko A. A. Monte Carlo simulation of the coagulation processes governed by Smoluchowski equation with random coefficients. *Monte Carlo Methods and Applications* (1997), **3**, No 4, 275–311.

[11] Sabelfeld K. K., Rogasinsky S. V., Kolodko A. A. and Levykin A. I. Stochastic algorithms for solving Smoluchowsky coagulation equation and applications to aerosol growth simulation. *Monte Carlo Methods and Applcations* (1996), **2**, No 1, 41–87.

[12] Saffman P. and Turner J.S. On the collision of drops in turbulent clouds. *J. Fluid Mech.* (1956), **1**, 16–30.

[13] Williams M.M.R. and Loyalka S.K. *Aerosol Science.Theory and Practice.* Pergamon, New York, 1991.

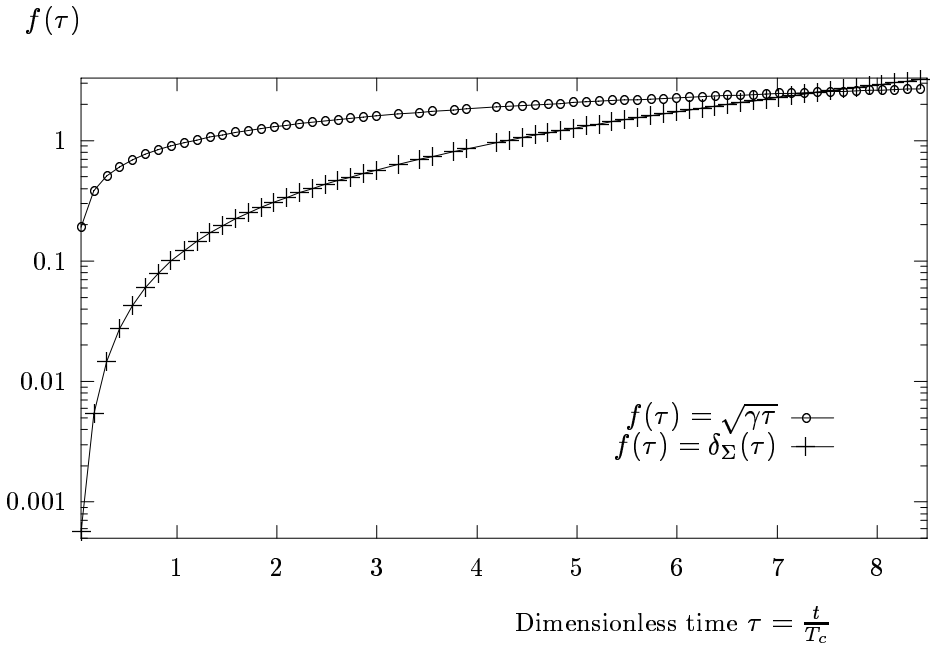

Fig.1. The relative difference $\delta_\Sigma(\tau)$ between the expectation of the total number of clusters in stochastic and deterministic cases. The coagulation rate $\gamma = 0.86$.

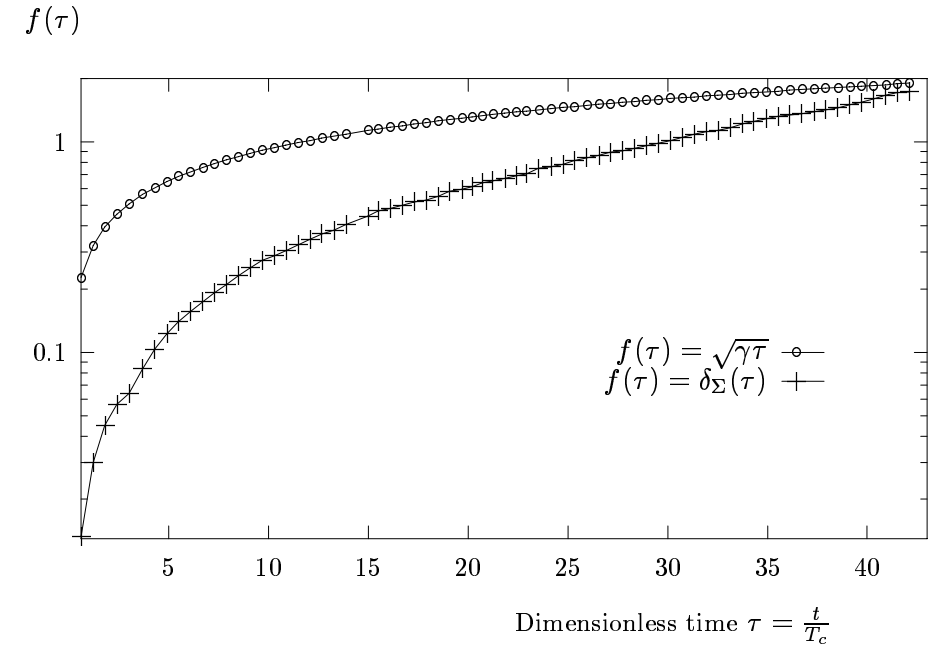

Fig.2. The same as in Fig.1, for $\gamma = 0.086$.

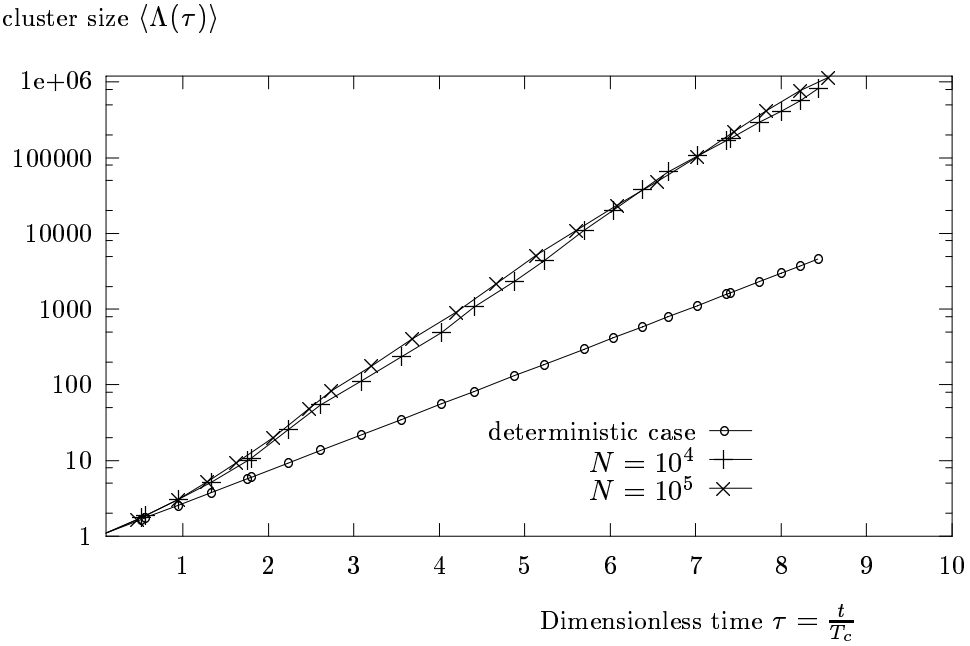

Fig.3. The expectation of the mean cluster size $\langle \Lambda(\tau) \rangle$ in stochastic ($N = 10^4$ and $N = 10^5$ samples) and deterministic cases; moderate high coagulation rate ($\gamma = 0.86$).

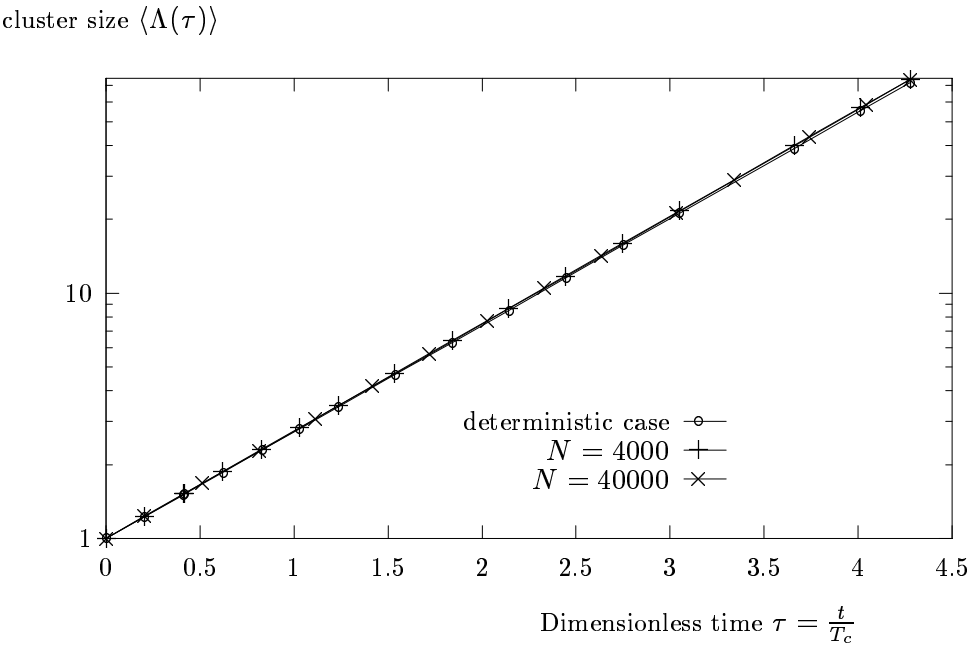

Fig.4. As in Fig.3, but for $\gamma = 0.0086$

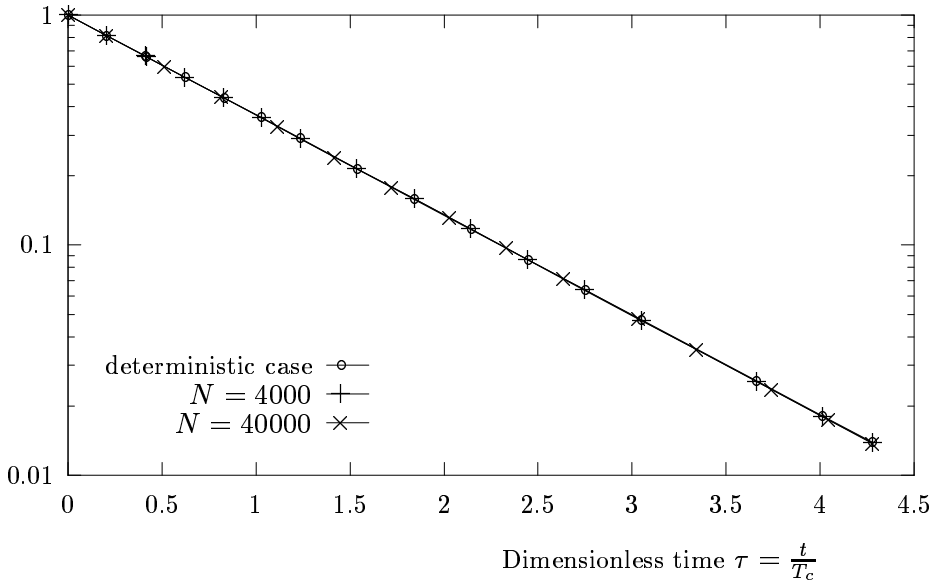

Fig.5. The total number of clusters $\langle \Sigma(\tau) \rangle$ for $\gamma = 0.0086$.

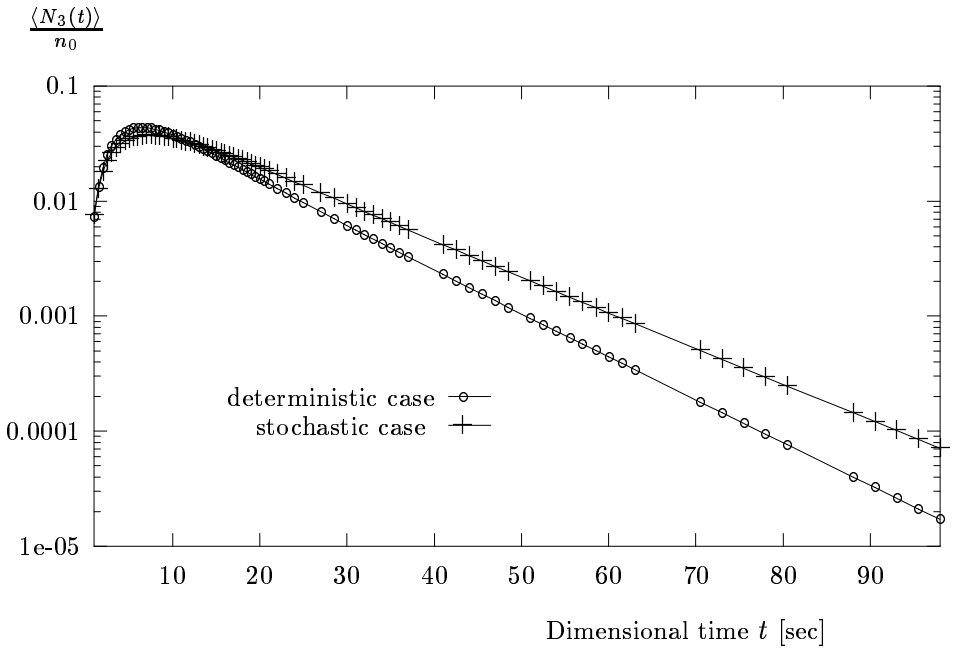

Fig.6. Concentration of 3-mers as a function of time; $\gamma = 0.86$.

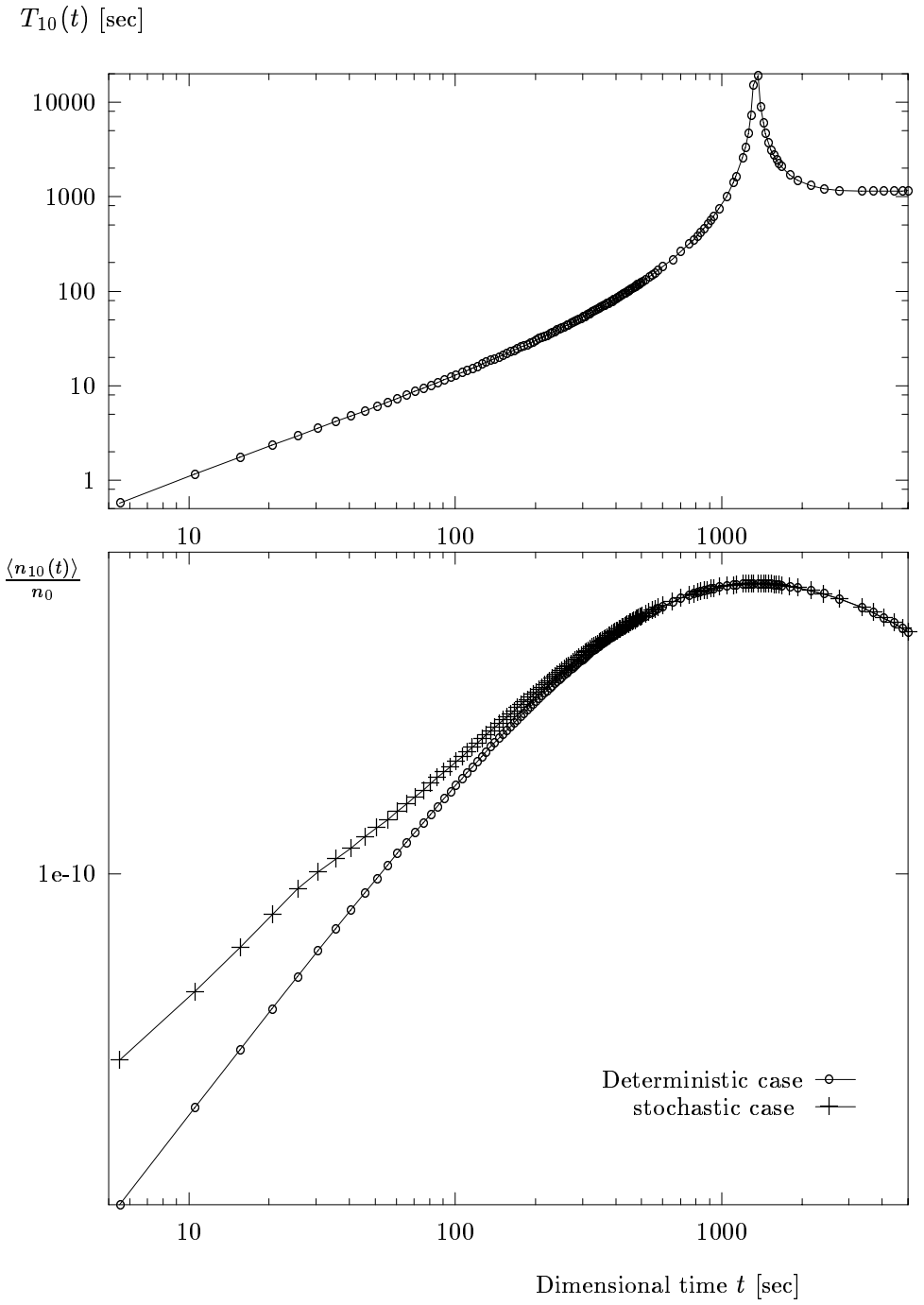

Fig.7. The concentration of 10-mers (lower picture) for stochastic and deterministic cases, $\gamma = 0.0086$ and the characteristic time scale $T_{10}(t)$ (upper picture).

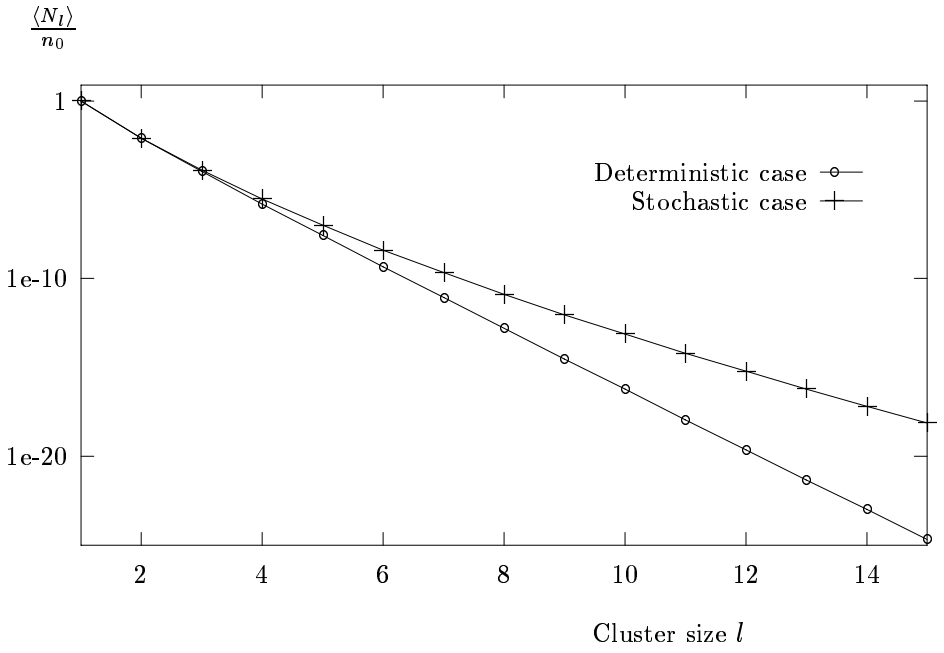

Fig.8. The size distribution for $\gamma = 0.0086$ at the time instant $t = T_w = 10$ sec.

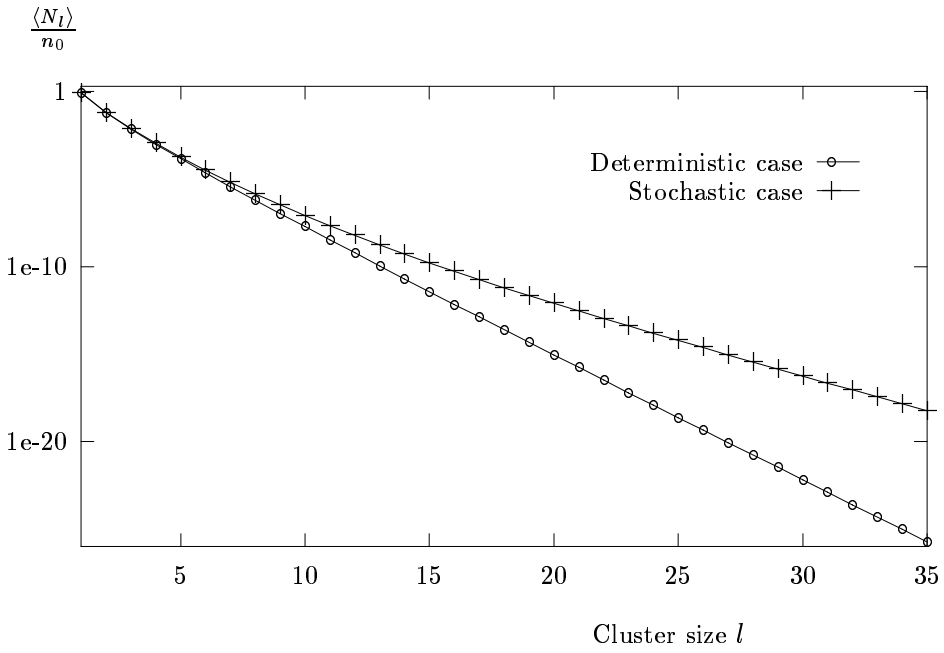

Fig.9 The same as in Fig.8, for $t = 10T_w = 100$ sec.

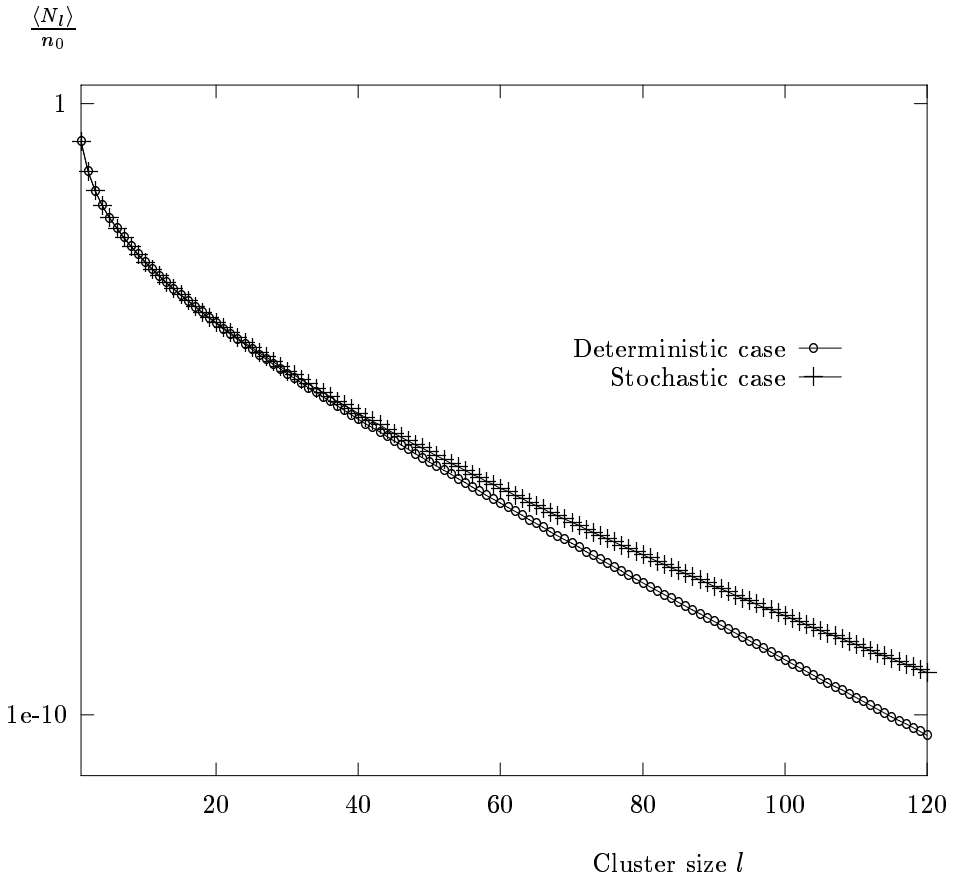

Fig.10. The same as in Fig.8, but for $t = 100T_w = 1000$ sec.

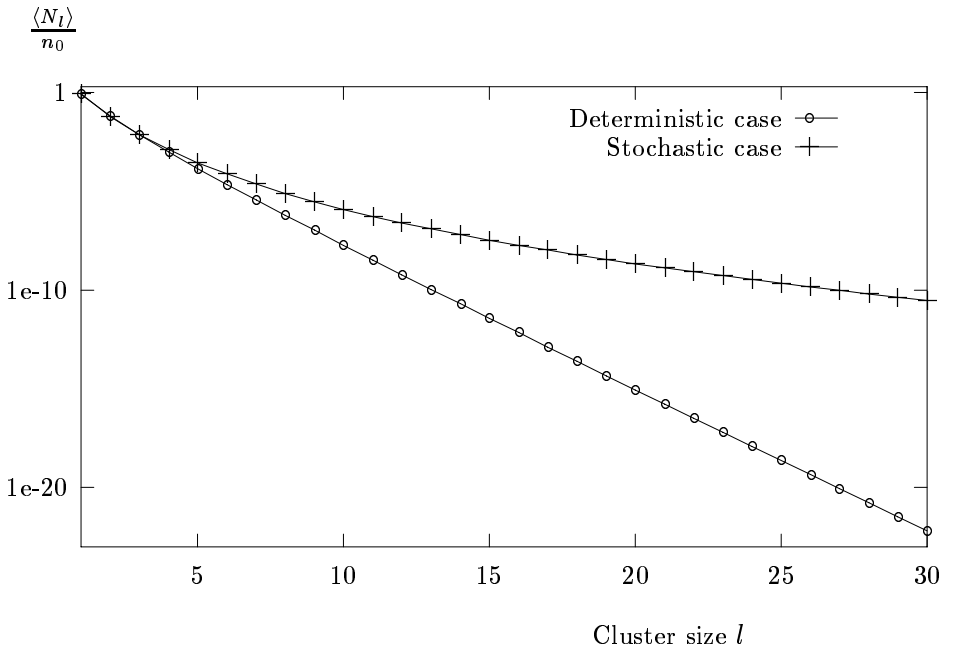

Fig.11. The size distribution for moderate slow coagulation rate ($\gamma = 0.086$) at the time instant $t = T_w = 10$ sec.

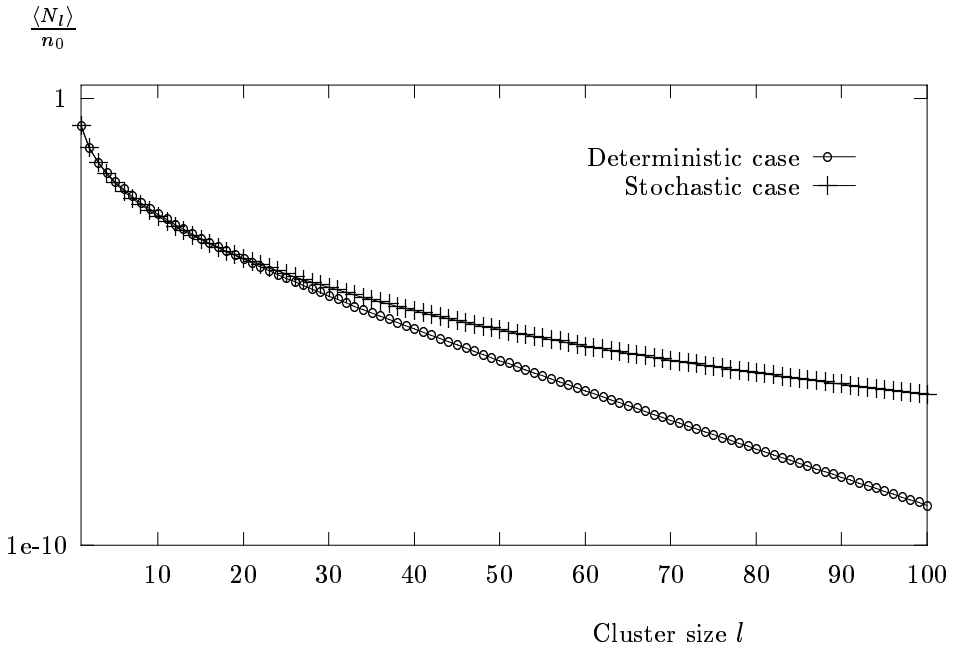

Fig.12. The same as in Fig.11, but for $t = 10T_w = 100$ sec.

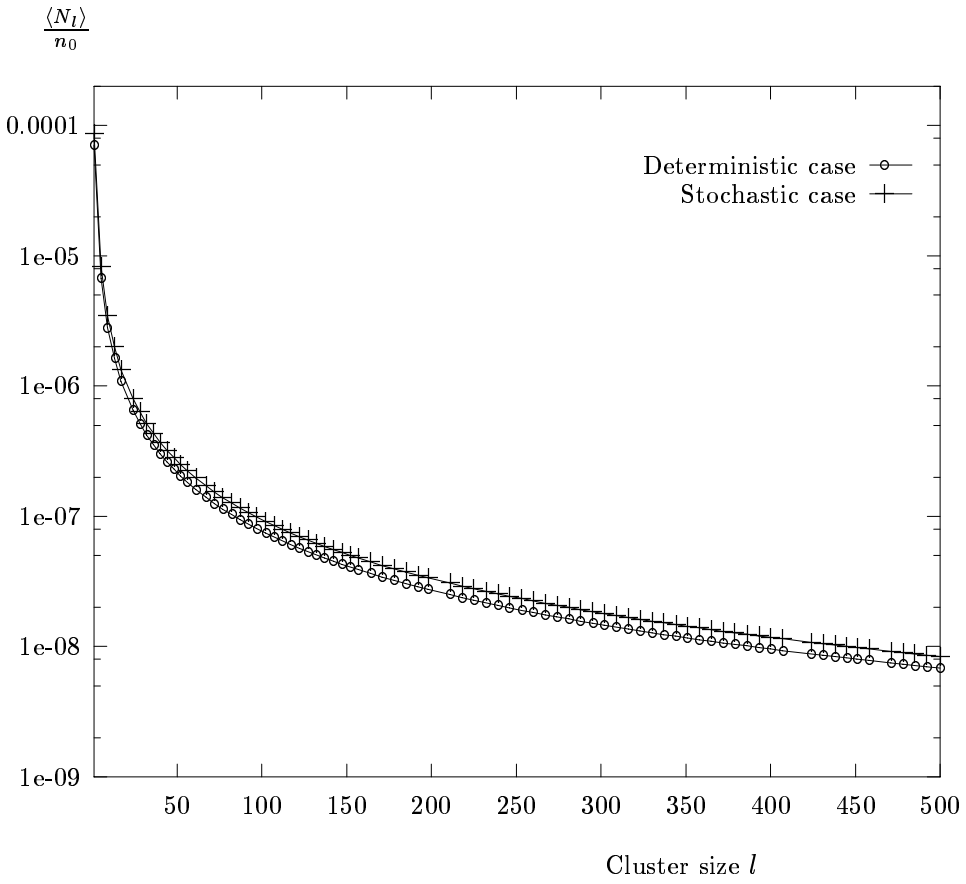

Fig.13. The same as in Fig.11, but for $t = 100T_w = 1000$ sec.

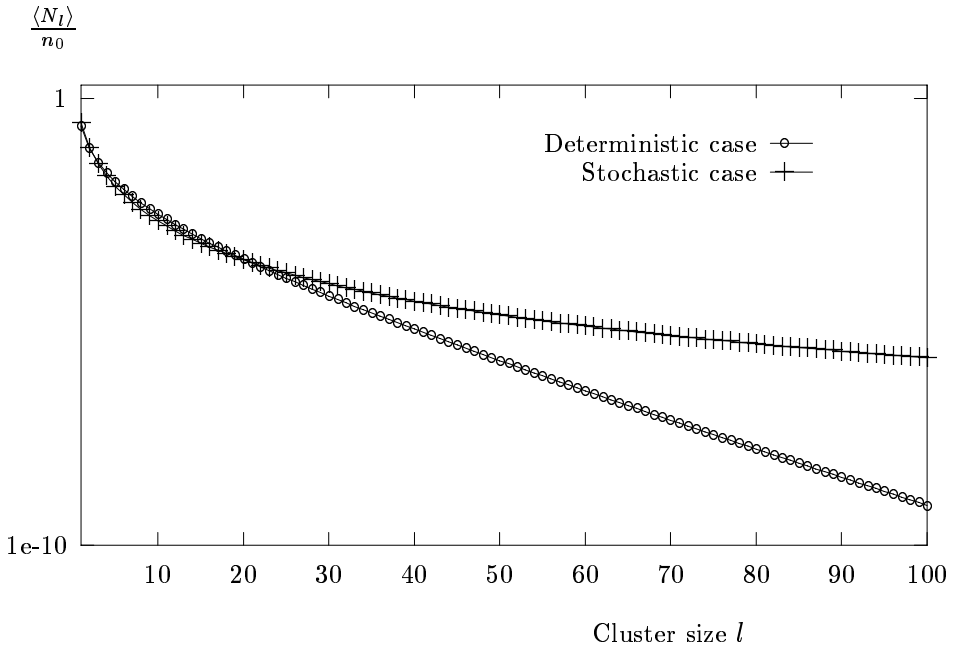

Fig.14. The size distribution for $\gamma = 0.86$ at $t = T_w = 10$ sec.

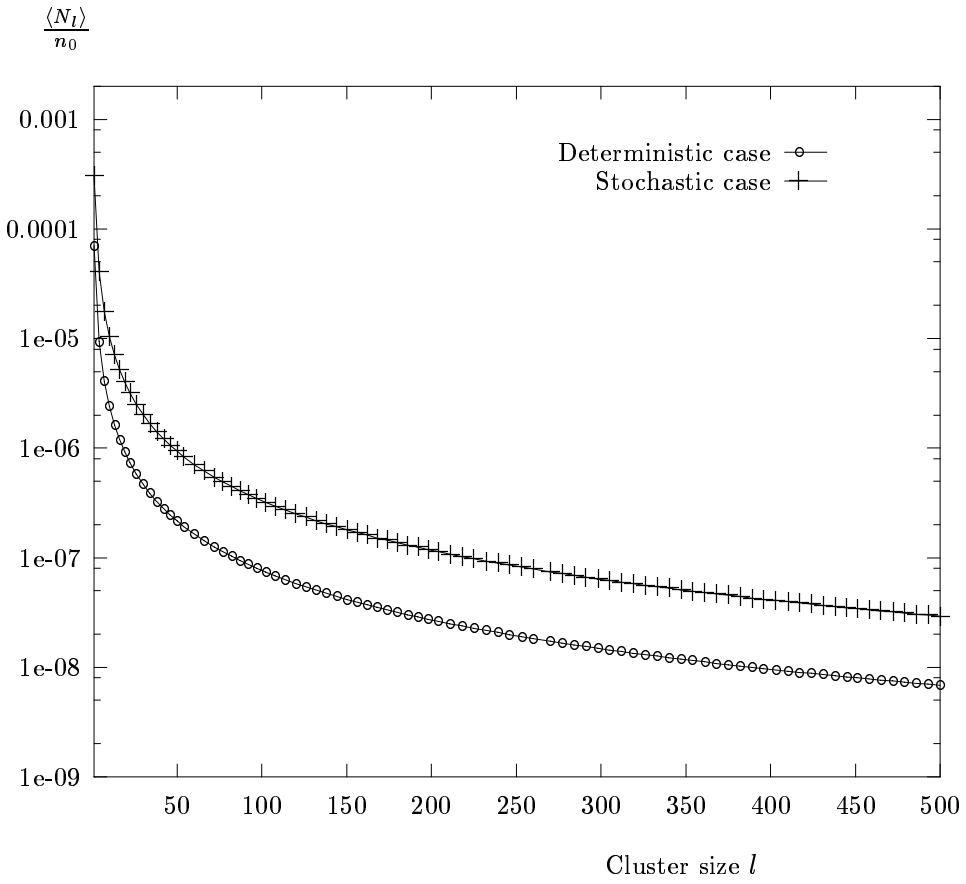

Fig.15. The same as in Fig.14, but for $t = 10T_w = 100$ sec.

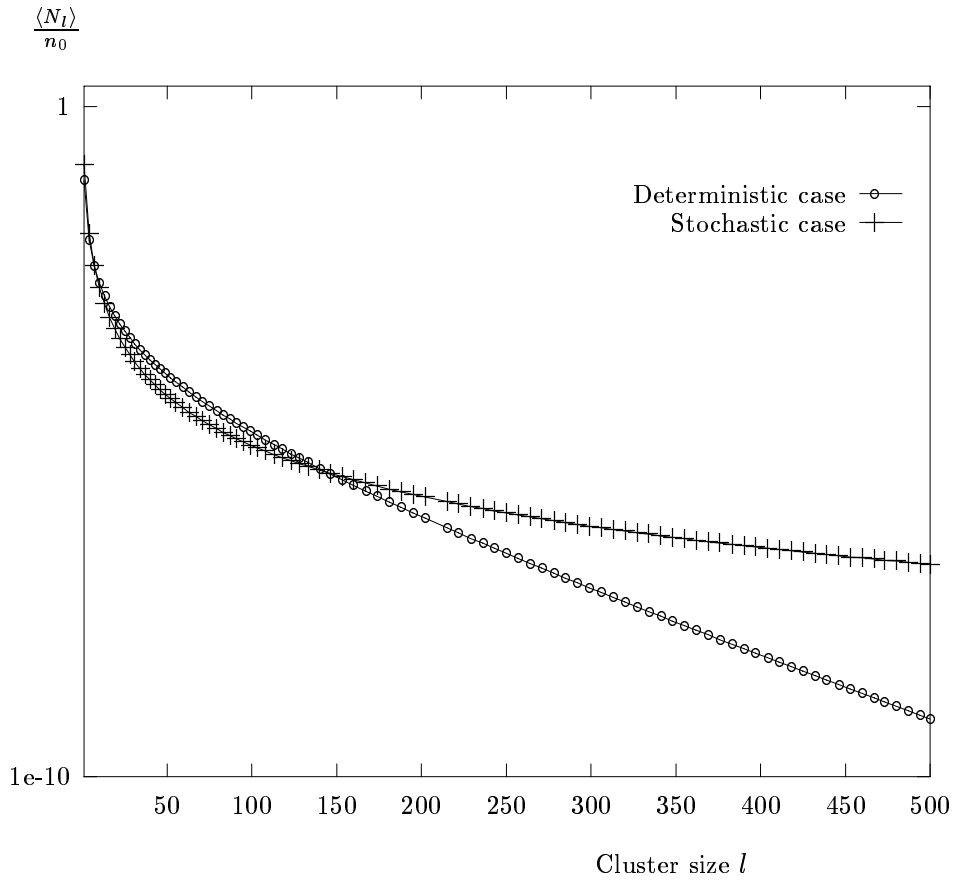

Fig.16. The size distribution for the high coagulation rate ($\gamma = 8.56$) at $t = 0.2T_w = 2$ sec.

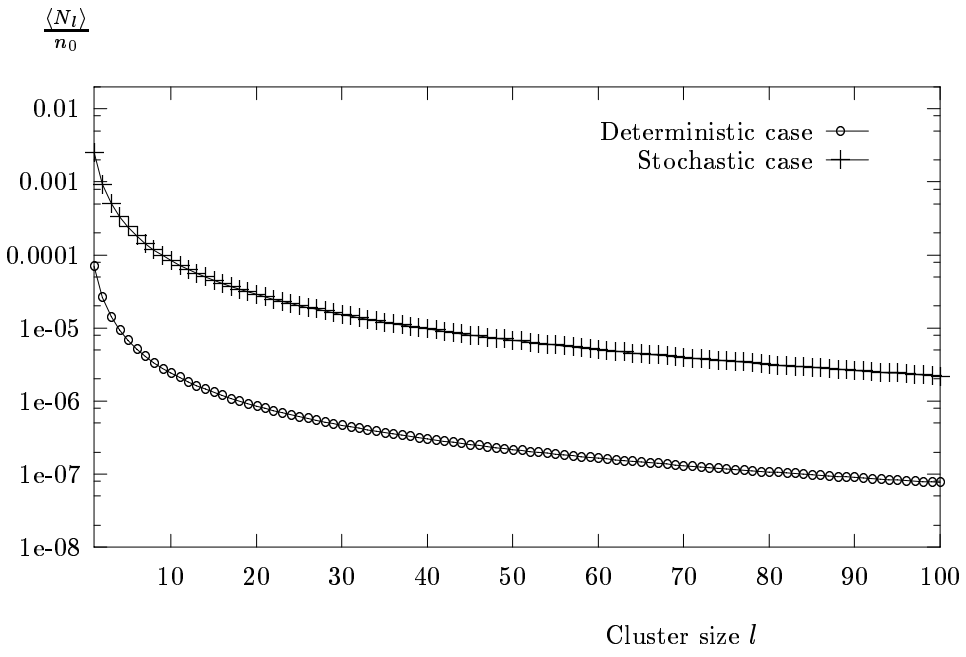

Fig.17. The same as in Fig.17, but for $t = T_w = 10$ sec.

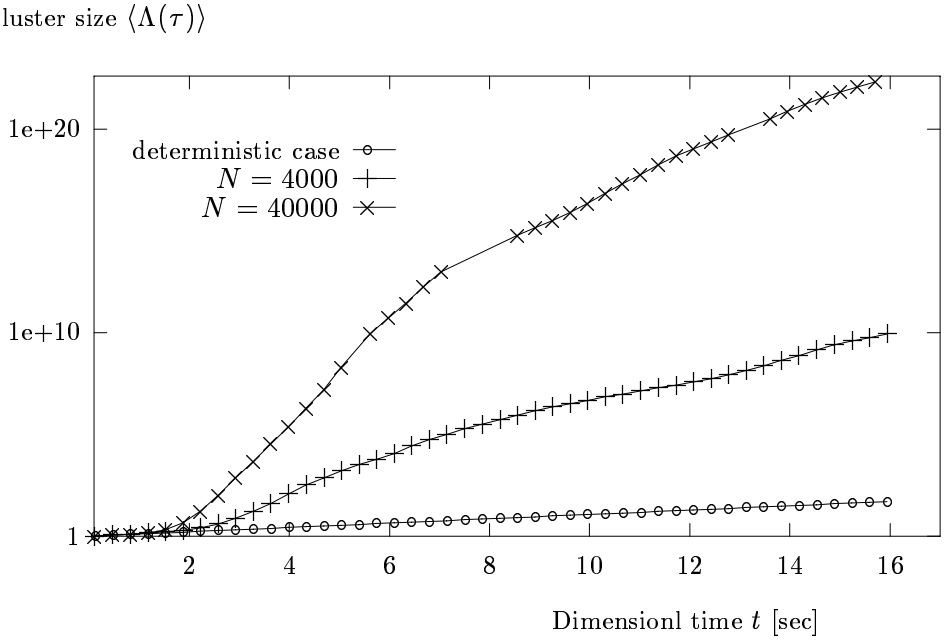

Fig.18. The expectation of the mean cluster size; the $P\&Ch$ model of energy dissipation rate. The case of high coagulation rate ($\gamma \sim 8$); $T_w = 30$ sec, $T_c = 4.05$ sec.

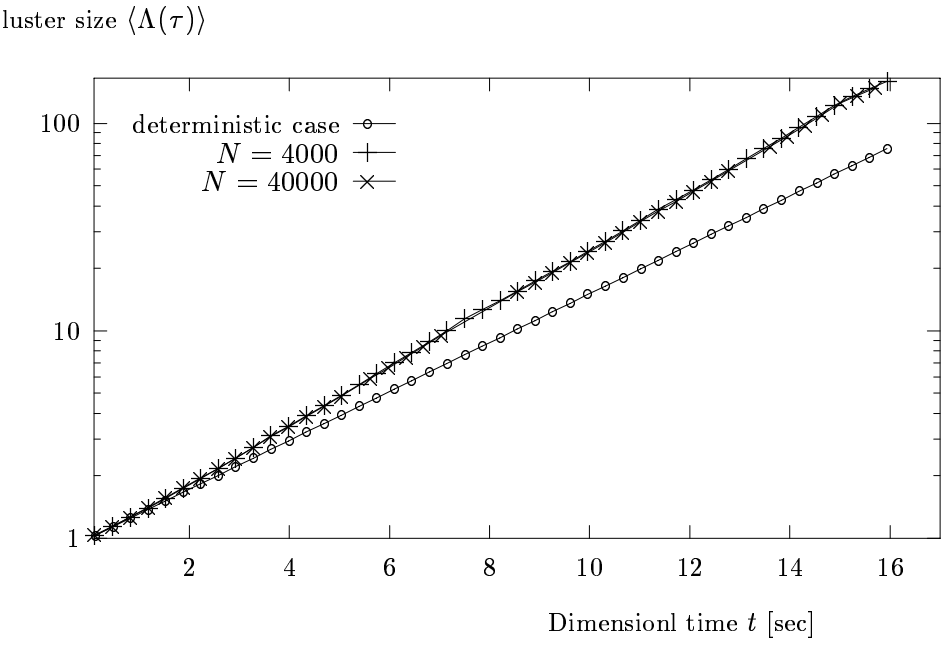

Fig.19. The same as in Fig.18, but for $B\&S$ model; the high coagulation rate ($\gamma \sim 8$); $T_w = 30$ sec, $T_c = 3.68$ sec.

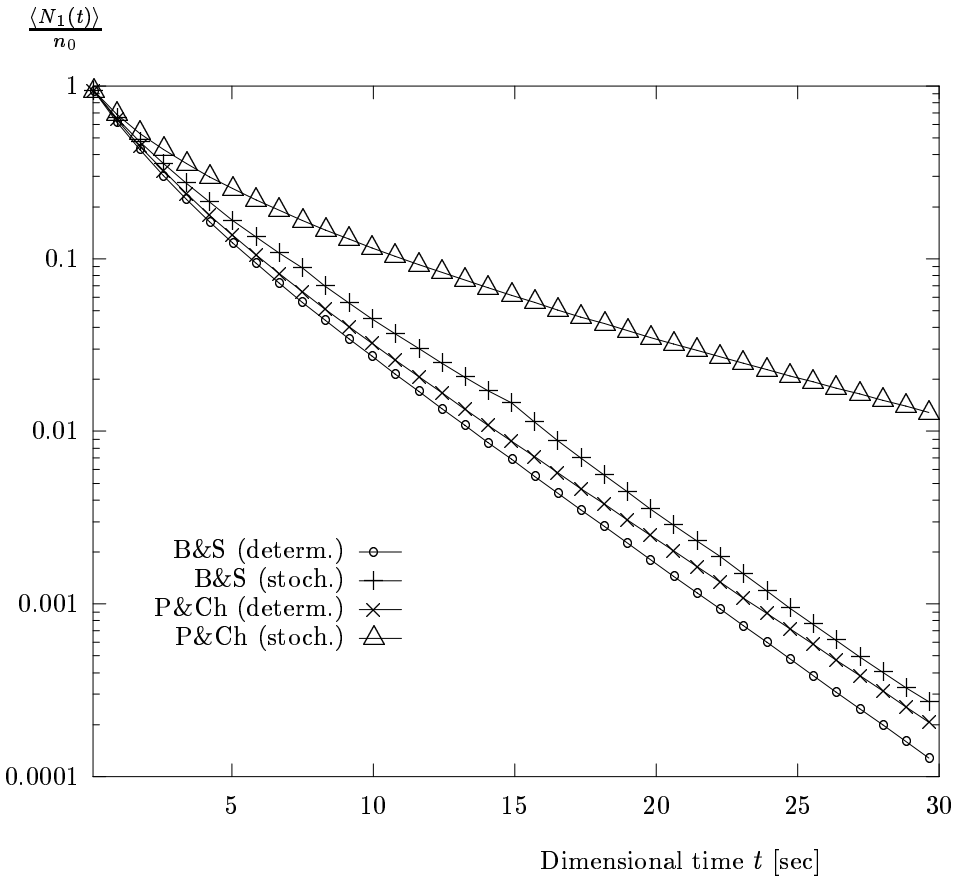

Fig.20. The monomer concentartion as a function of time, for high coagulation rate ($\gamma \sim 8$). Comparison of $P\&Ch$ and $B\&S$ models.

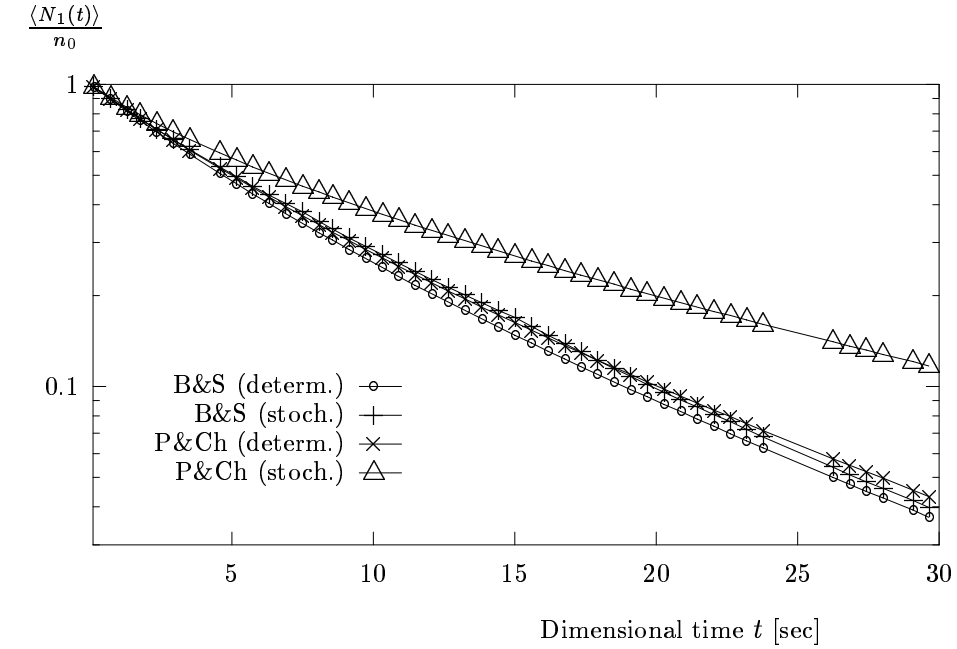

Fig.21. The same as in Fig.20, but for the moderate high coagulation rate ($\gamma \sim 2.5$); $T_c(B\&S) = 12.41$ sec, $T_c(P\&Ch = 13.2$ sec.

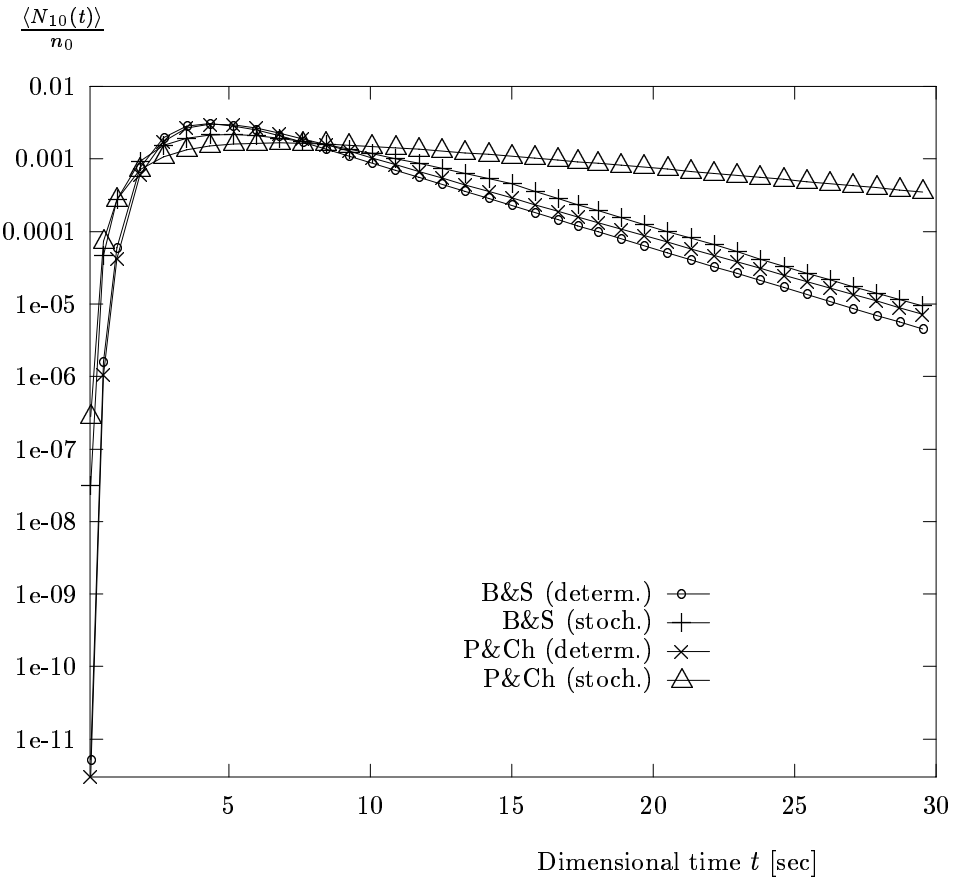

Fig.22. The concentartion of 10-mers as a function of time, for high coagulation rate ($\gamma \sim 8$). Comparison of $P\&Ch$ and $B\&S$ models.

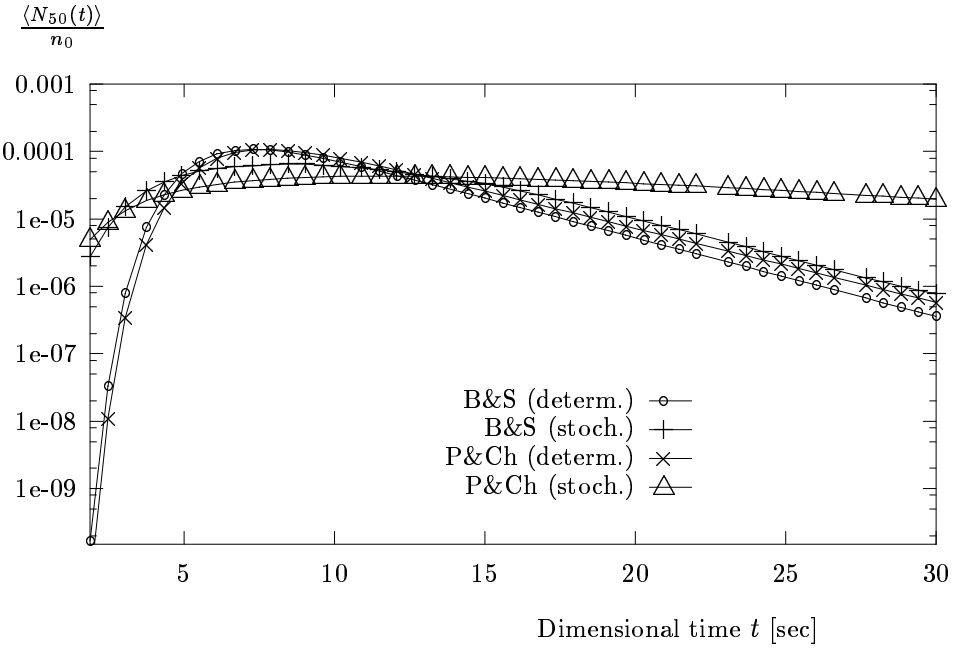

Fig.23. The same as in Fig.22, but for 50-mers.

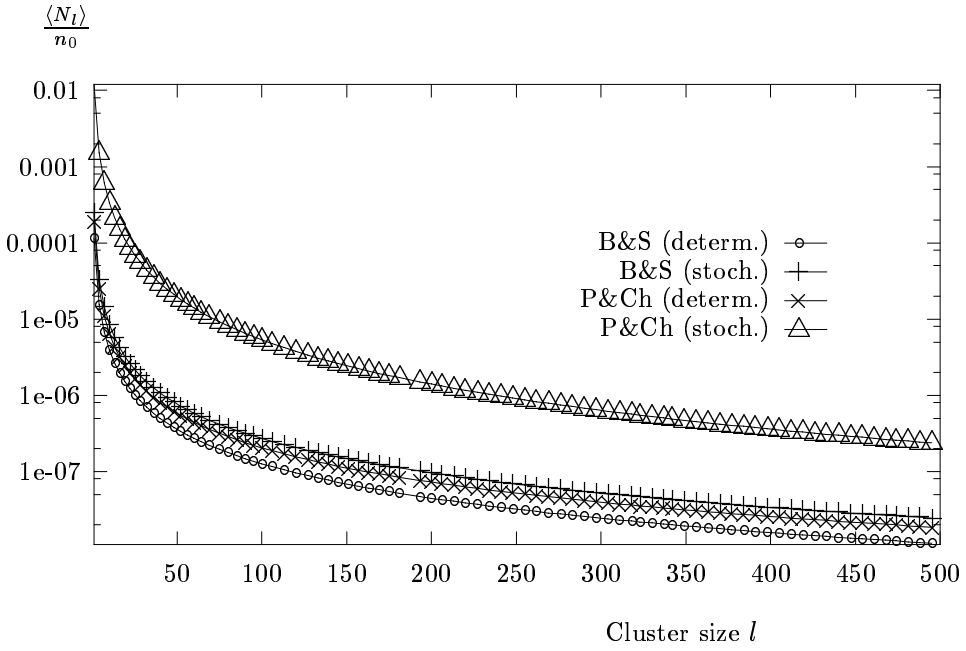

Fig.24. The size spectrum at the time $t = T_w = 30$ sec, for high coagulation rate ($\gamma \sim 8$). Comparison of $P\&Ch$ and $B\&S$ models.

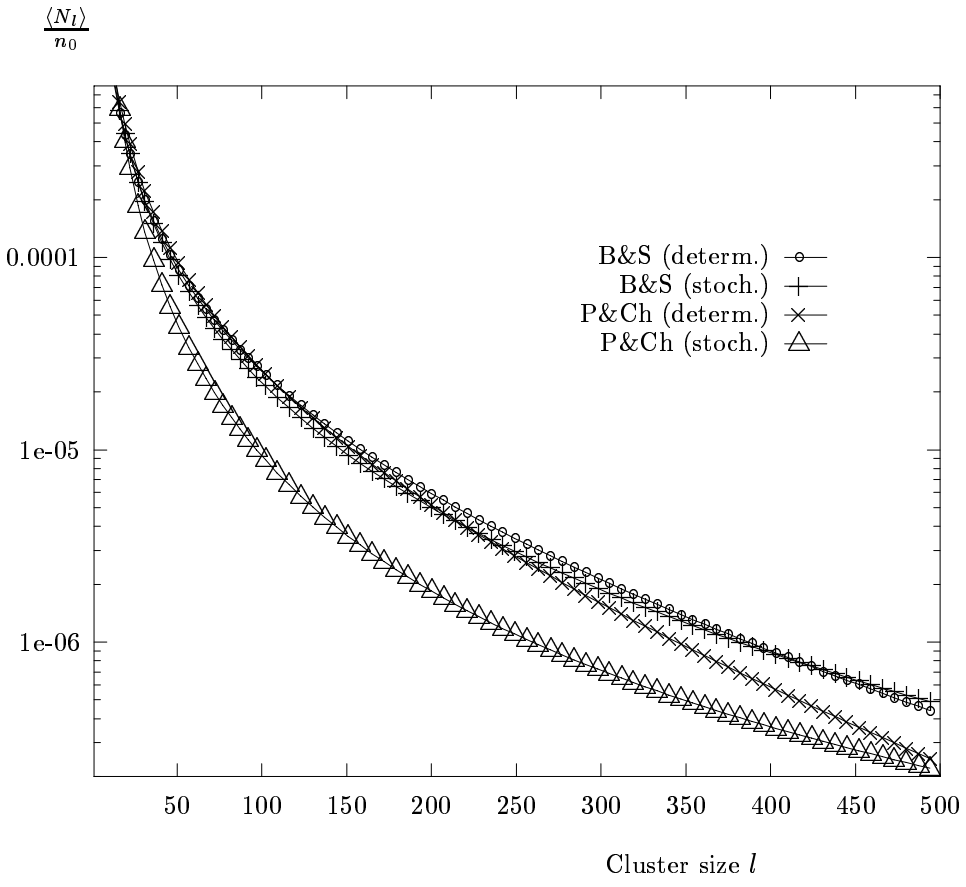

Fig.25. The same as in Fig.24, but for the moderate high coagulation rate ($\gamma \sim 2.5$).

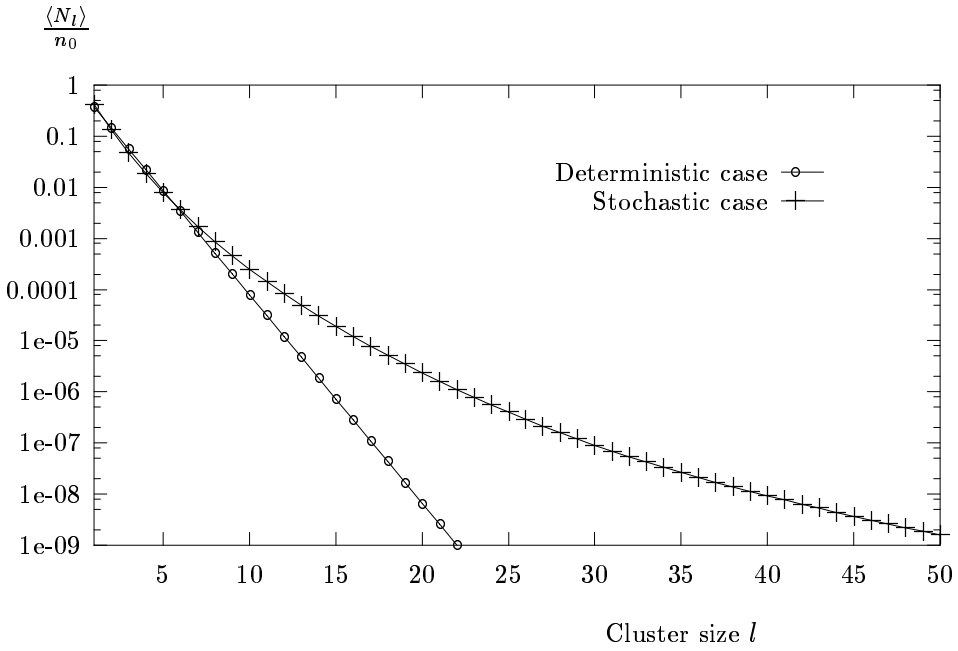

Fig.26. The size spectrum in the case of the coagulation coefficient (5.1); high coagulation rate ($\gamma \sim 10$), the time $t = 1.5$ sec, $T_w = 10$ sec. $T_c = 1.16$ sec.

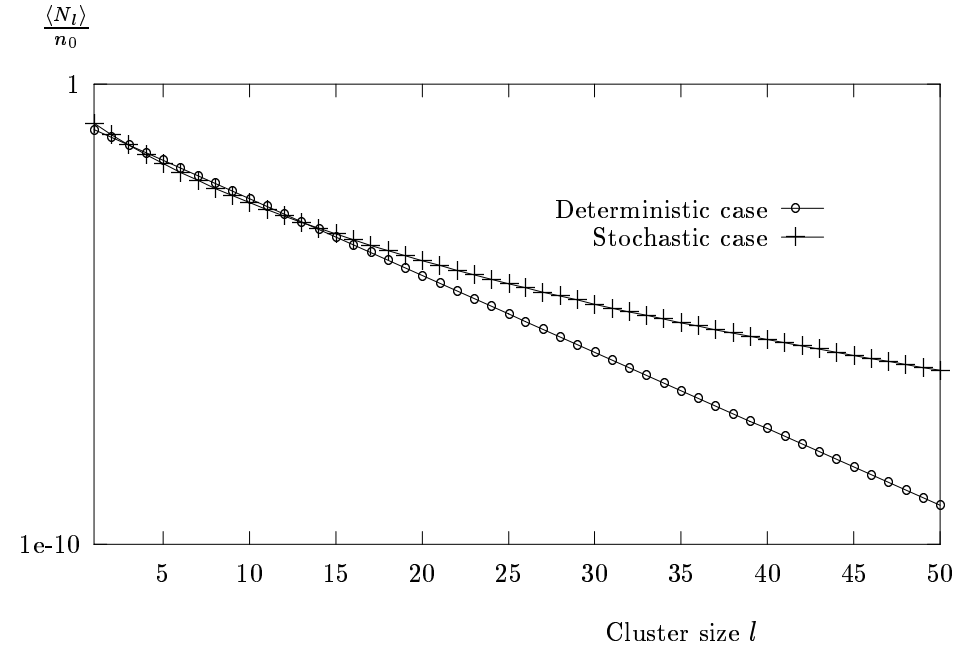

Fig.27. The same as in Fig.26, but for $t = 5$ sec.

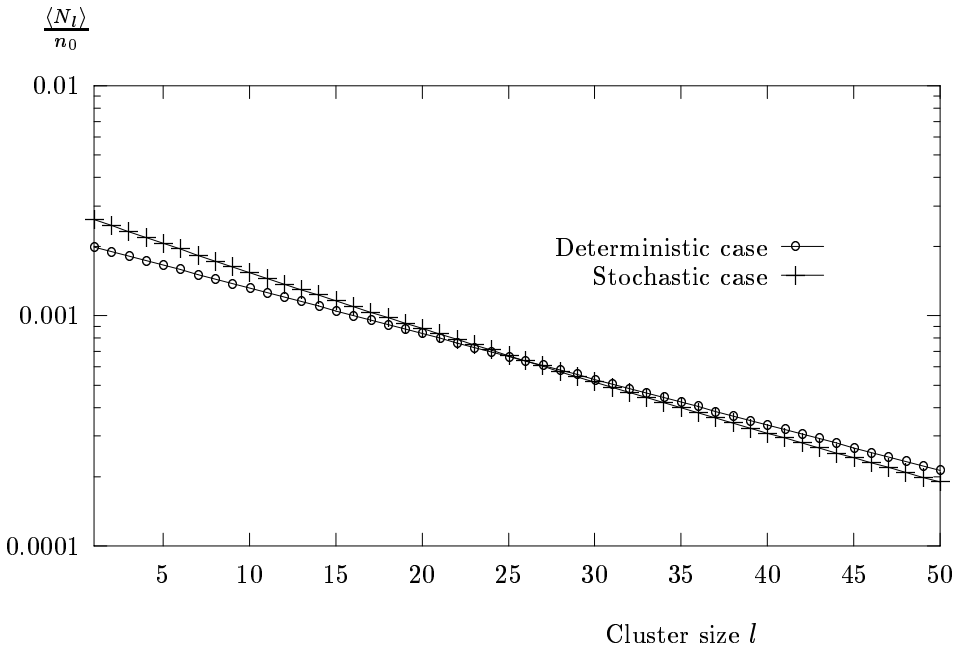

Fig.28. The same as in Fig.26, but for high coagulation rate ($\gamma \sim 10$, $T_w = 10$ sec, $T_c = 1.16$ sec) at the time $t = 50$ sec.

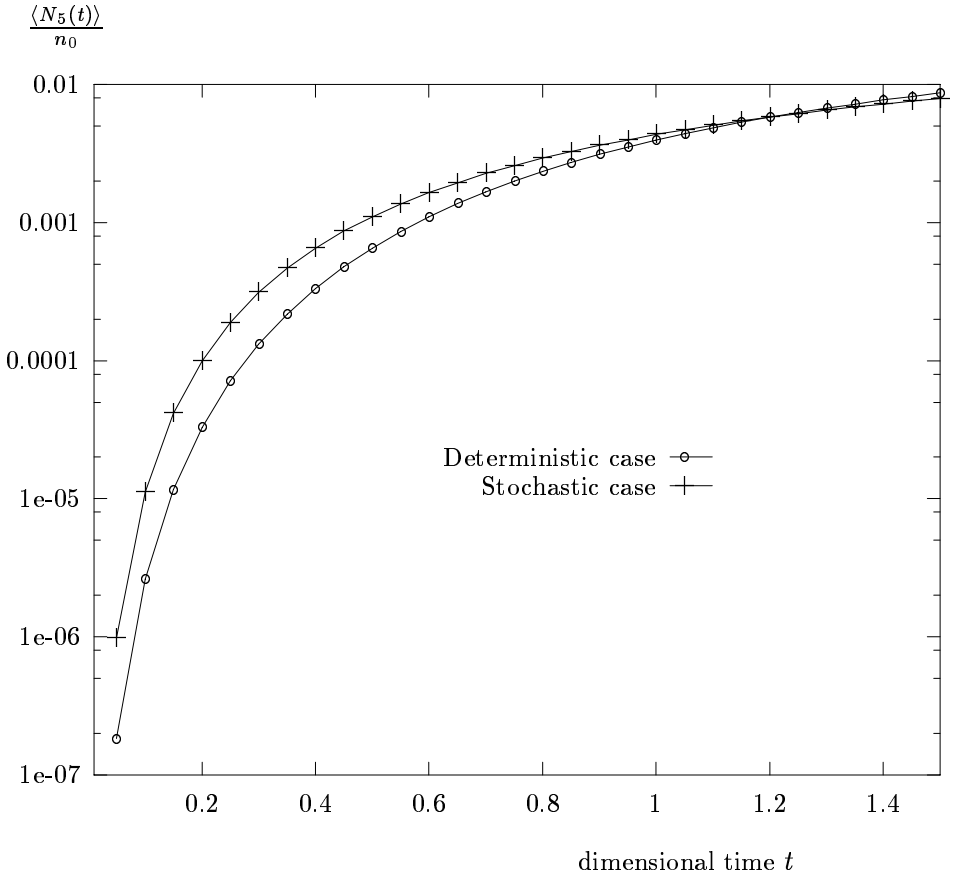

Fig.29. The concentartion of 5-mers as a function of time, for the case of the coagulation coefficient (5.1) ; high coagulation rate ($\gamma \sim 10$), $T_w = 10$ sec.

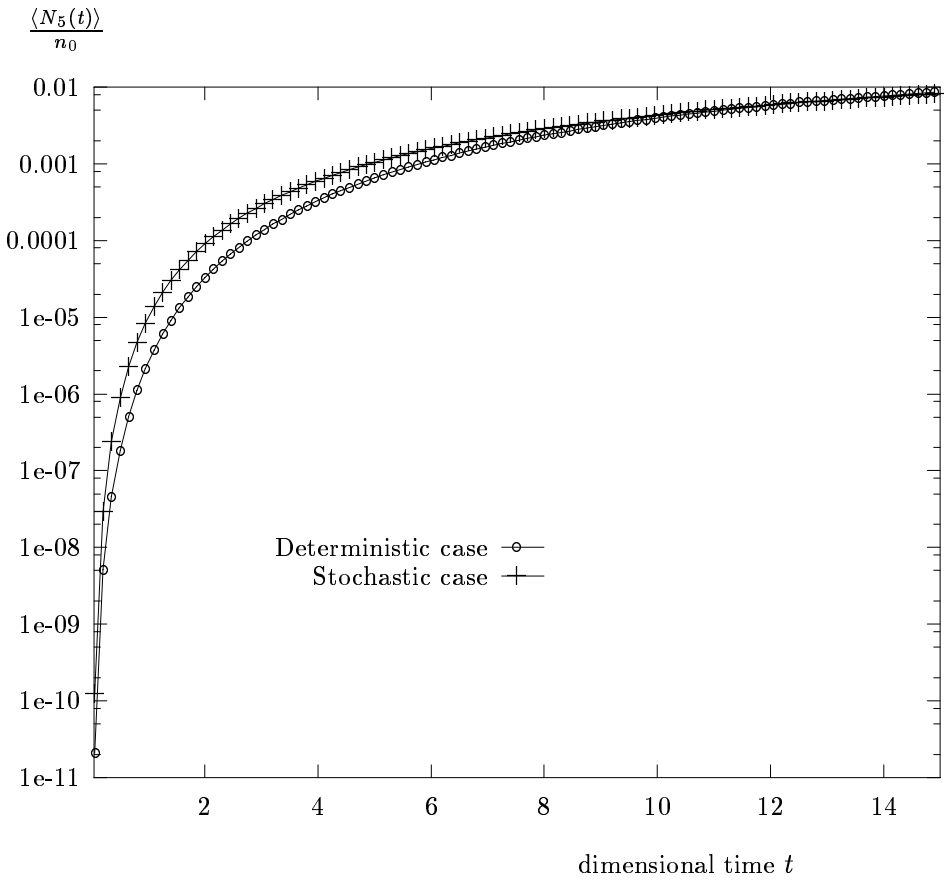

Fig.30. The same as in Fig.29, but for moderate high coagulation rate ($\gamma \sim 1$, $T_w = 10$ sec, $T_c = 11.68$ sec).

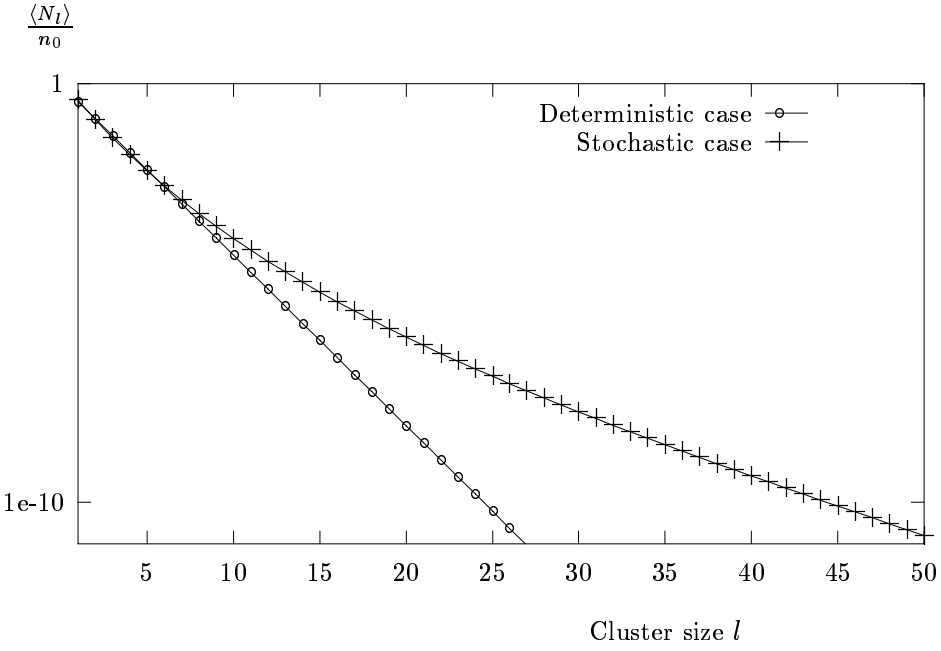

Fig.31. The same as in Fig.26, but for moderate high coagulation rate ($\gamma \sim 1$, $T_w = 10$ sec, $T_c = 11.68$ sec), at the time $t = 15$ sec.

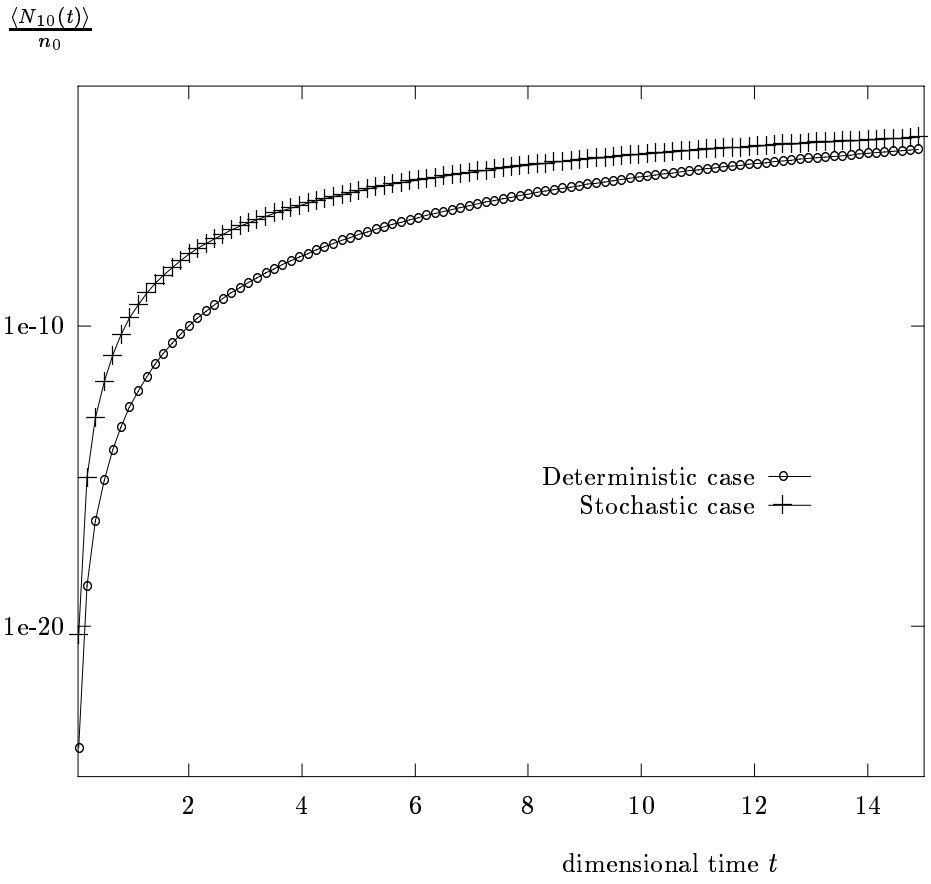

Fig.32. The same as in Fig.29, but for 10-mers, for moderate high coagulation rate ($\gamma \sim 1$, $T_w = 10$ sec, $T_c = 11.68$ sec).

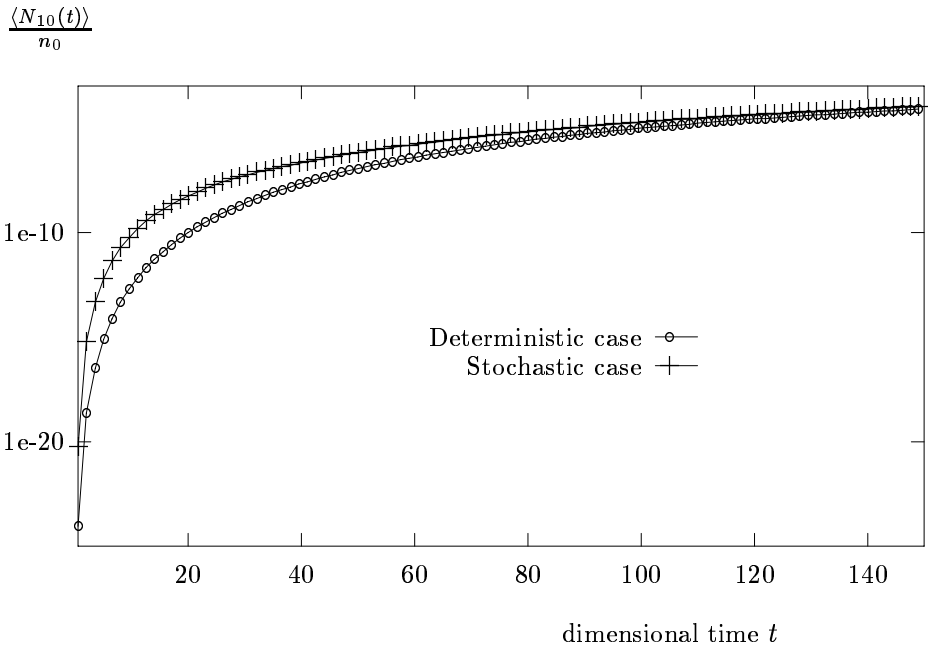

Fig.33. The same as in Fig.29, but for 10-mers, for moderate low coagulation rate ($\gamma \sim 0.1$, $T_w = 10$ sec, $T_c = 116$ sec).

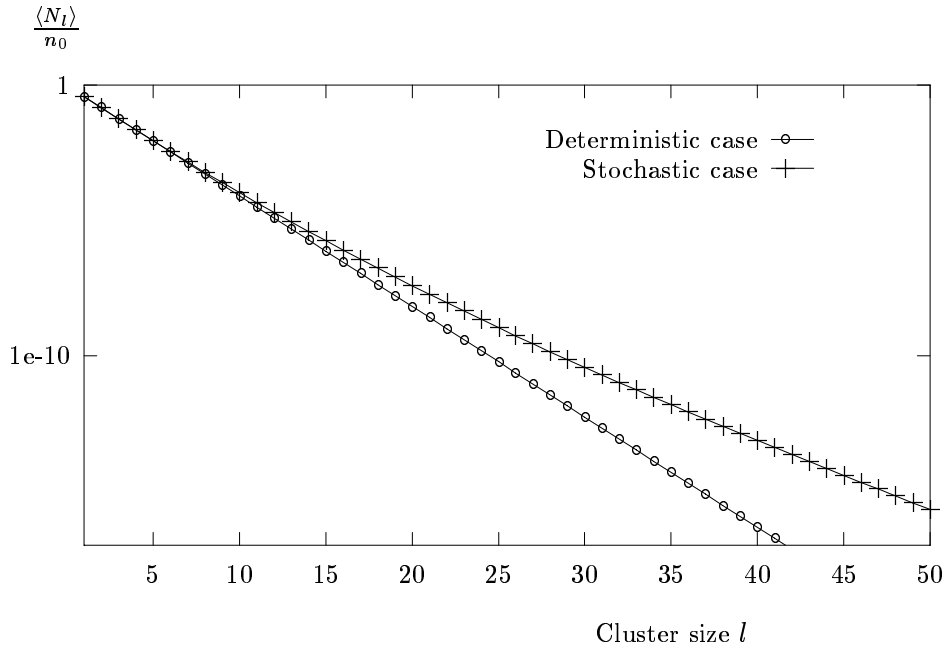

Fig.34. The same as in Fig.26, but for moderate low coagulation rate ($\gamma \sim 0.1$, $T_w = 10$ sec, $T_c = 116$ sec) at the time $t = 150$ sec.

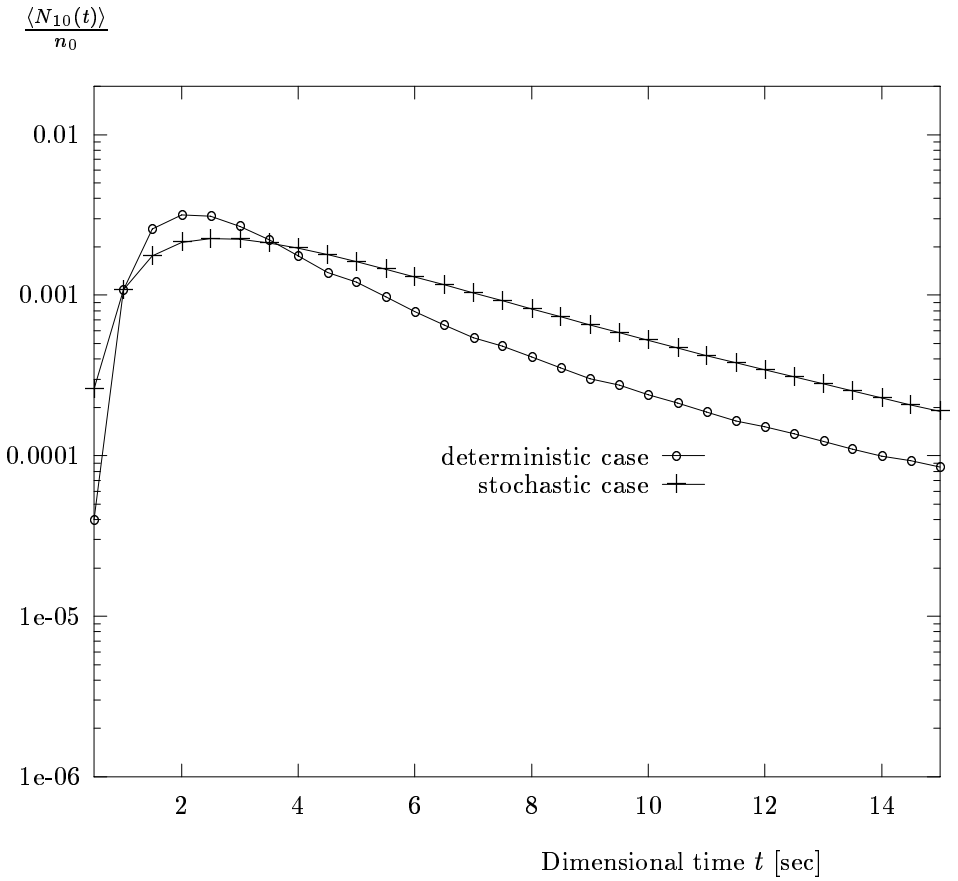

Fig.35. The concentartion of 10-mers as a function of time, for the case of turbulent coagulation regime (6.1); high coagulation rate ($\gamma \sim 11$).

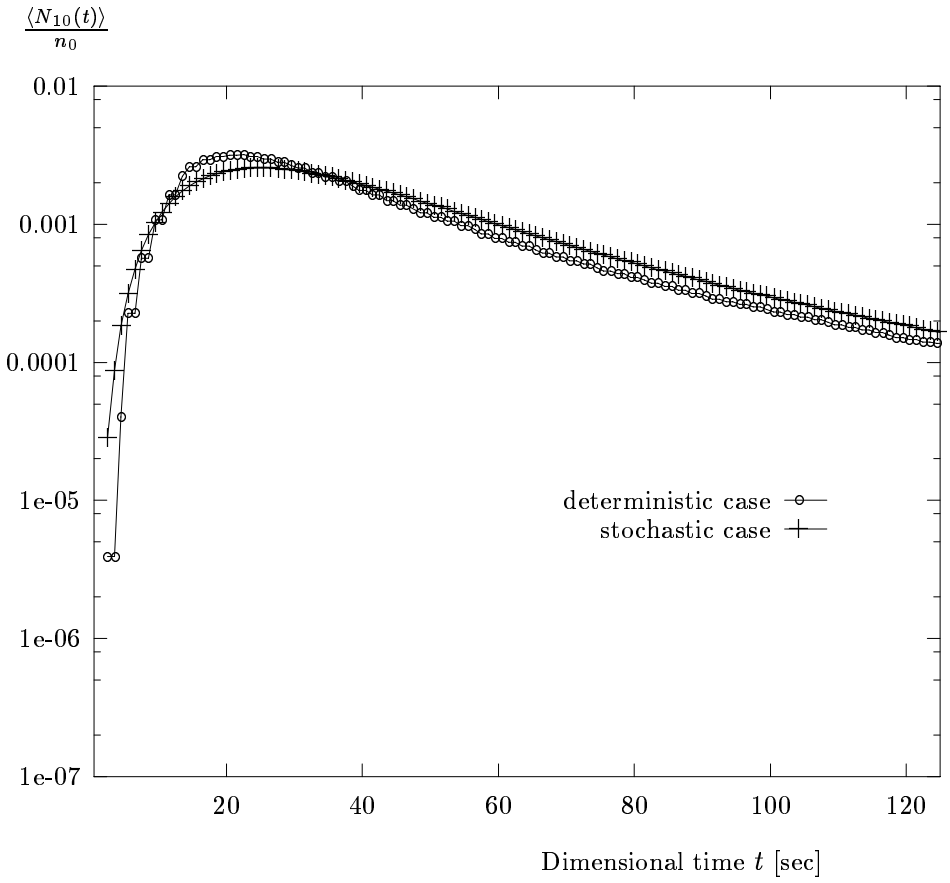

Fig.36. The same as in Fig.35, but for $\gamma \sim 1$.

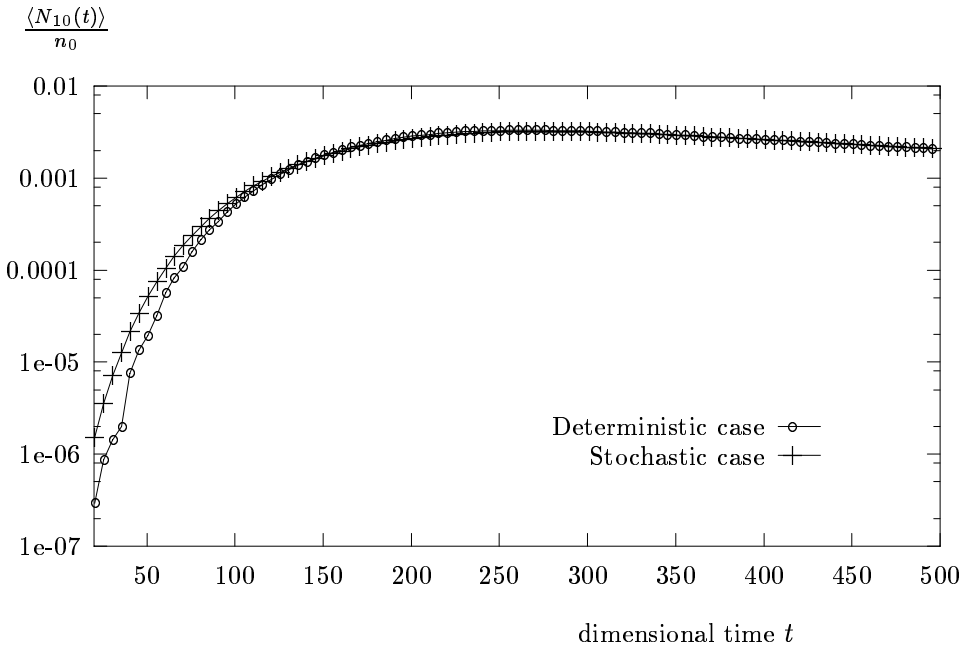

Fig.37. The concentartion of 10-mers as a function of time, for the case of corrected turbulent coagulation coefficient (6.2); moderate low coagulation rate ($\gamma \sim 0.1$).

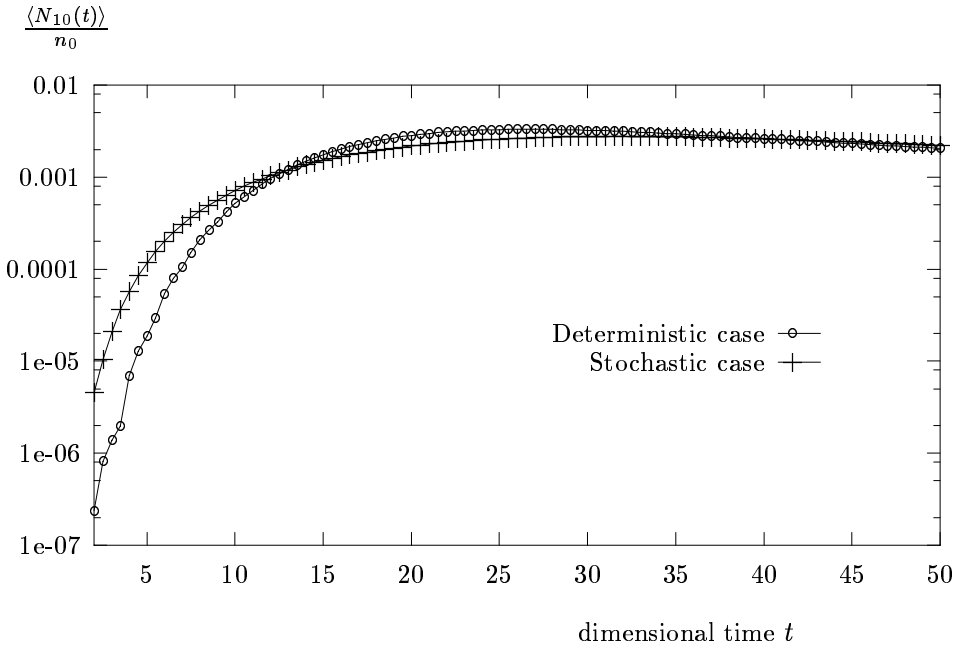

Fig.38. The same as in Fig.37, but for the moderate high coagulation rate ($\gamma \sim 1.1$).

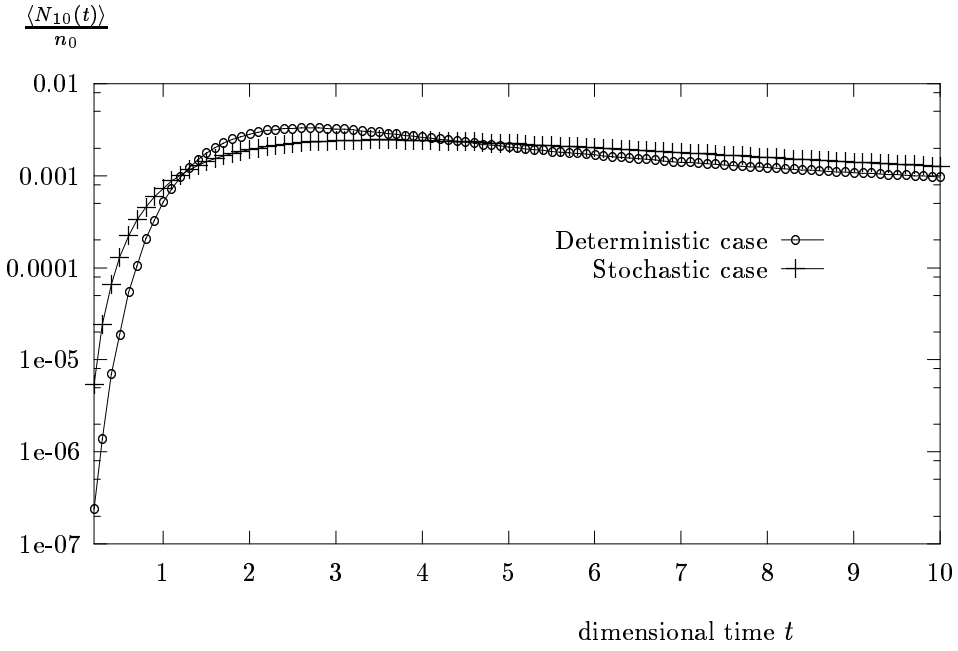

Fig.39. The same as in Fig.37, but for the high coagulation rate ($\gamma \sim 11$).